Article

Not peer-reviewed version

Reverse Vaccinology and Immune Simulation of a Novel Multiepitope Vaccine Targeting *Brucella* Virulence

Mostafa F. Abushahba *

Posted Date: 3 December 2025

doi: 10.20944/preprints202512.0403.v1

Keywords: *Brucella*; zoonosis; vaccine; epitope; vaccination; in silico; simulation; virulence; iron; genes

Article

Reverse Vaccinology and Immune Simulation of a Novel Multiepitope Vaccine Targeting *Brucella* Virulence

Mostafa F. Abushahba [1,2,3]

[1] Department of Veterinary Pathobiology, College of Veterinary Medicine, University of Missouri, Columbia, Missouri, USA

[2] Laboratory for Infectious Disease Research, University of Missouri, Columbia, Missouri, USA

[3] Department of Zoonoses, Faculty of Veterinary Medicine, Assiut University, Assiut, Egypt

* Correspondence: mostafaa@missouri.edu

Abstract

Background/Objectives: *Brucella* is a major global One Health threat, causing an estimated 2.1 million human infections and substantial livestock losses annually, with no vaccine currently available for humans, underscoring the urgent need for a safe and effective vaccine. **Methods**: Employing a reverse vaccinology approach, a novel 175-mer multiepitope vaccine (Mvax) targeting *Brucella* FrpB was computationally designed in this study, incorporating two B-cell, two MHC class I (MHC-I), and three MHC class II (MHC-II) epitopes selected for their high predicted antigenicity, safety, and IFN-γ-inducing potential. To further enhance immune activation, human beta-defensin-3 was fused to the N-terminus as an adjuvant, followed by comprehensive in silico evaluation of the construct. **Results**: Population coverage analysis showed the selected epitopes provide 99.59% global coverage for MHC class combined, suggesting broad immunogenic potential. Mvax is predicted to be substantially more soluble (Protein-SOL score 0.808 vs. 0.275) with greater antigenicity (VaxiJen score 1.06 vs. 0.61) than native FrpB. Dissociation constant (Kd) analysis at 37ºC predicts stronger binding of Mvax to human TLR4/MD2 and TLR2/TLR6 receptors. Immune simulations (over 100 days and three years) indicate that a single dose of Mvax may elicit a strong Th1 response, generate durable T-cell memory lasting up to three years, and produce elevated IL-12, IFN-γ, and IL-2 levels, along with approximately ten-fold higher IgM responses compared with FrpB. **Conclusions**: In silico data from this study suggest that Mvax could serve as a safe and effective vaccine candidate for human brucellosis, with the potential to induce long-lasting immune memory; however, experimental validation is still required.

Keywords: *Brucella*; zoonosis; vaccine; epitope; vaccination; in silico; simulation; virulence; iron; genes

Introduction

Brucellosis, one of the most common bacterial zoonosis globally, results from infection with non-motile, Gram-negative *Brucella* organisms that persist as facultative intracellular pathogens [1,2]. Among the numerous *Brucella* species identified to date, three are highly virulent for both their natural hosts and humans and remain endemic in most countries, particularly in resource-limited settings [1]. These are *B. melitensis*, which primarily infects sheep and goats; *B. suis*, which mainly infects swine; and *B. abortus*, which primarily infects cattle [3]. Human infection primarily occurs through direct contact with infected animals or tissues, consumption of contaminated unpasteurized dairy products or undercooked meat, and inhalation of infectious aerosols in occupational settings like labs or abattoirs [4–6]. The global burden of human brucellosis has increased dramatically in recent years, with current estimates indicating approximately 2.1 million new cases annually

 doi:10.20944/preprints202512.0403.v1

worldwide [1]. Africa and Asia bear the majority of this risk and caseload, though regions in the Americas and Europe remain of concern [1].

Chronic brucellosis can occur despite appropriate treatment, with relapses ranging from 5-30% after therapy cessation, causing symptoms such as fatigue, joint pain, and depression [7,8]. Within macrophages and dendritic cells, the pathogen disrupts intracellular trafficking, delays lysosomal fusion, and manipulates host signaling to establish a permissive niche, allowing replication without host cell destruction and sustaining low-grade chronic inflammation [9]. Emerging research also implicates B cells in disease chronicity [10–12]. Similar to other intracellular pathogens, such as *Mycobacterium*, *Salmonella*, and *Listeria*, *Brucella* presents major therapeutic challenges due to the limited ability of most antibiotics to penetrate host cells and effectively reach its intracellular niches [13].

Despite decades of research, there is still no licensed vaccine for human brucellosis, posing significant challenges for disease control, particularly in endemic regions [8,14]. A primary challenge in developing an effective human *Brucella* vaccine lies in devising immunization strategies that elicit robust, long-lasting memory responses while ensuring complete safety [15]. Live attenuated *Brucella* vaccines are generally effective but raise significant safety concerns for human use [16]. Historically, attenuated strains such as *Brucella abortus* strain 19 (used in the Soviet Union) and strain 104M (tested in China) were administered to humans for brucellosis but were eventually discontinued due to safety concerns [17].

Subunit and DNA vaccines are under active preclinical investigation, demonstrating superior safety and promising Th1 immunogenicity as potential alternatives to live-attenuated vaccines [8]. Recent advances in reverse vaccinology offer powerful tools for identifying protective antigens, predicting immune-dominant epitopes, and rationally designing vaccine constructs with enhanced safety and efficacy [18]. These computational approaches enable researchers to prioritize virulence-associated proteins, optimize epitope combinations, and engineer vaccine candidates capable of eliciting strong and targeted immune responses [18]. Building on these innovations, next-generation optimized multiepitope vaccines that target key bacterial virulence factors could provide a promising path toward safer and more effective protection against *Brucella* infection [19–24].

As we previously evaluated the safety and efficacy of a green subunit *Brucella* vaccine in a mouse model [25] and characterized S19 vaccine-mediated immunity against *B. melitensis* [26], the present study builds on this foundation by proposing a novel in silico designed multiepitope vaccine targeting *Brucella* virulence. This vaccine was strategically constructed from highly antigenic epitopes with strong predicted binding affinity to immune receptors, derived from the multispecies *Brucella* iron-regulated outer membrane protein FrpB. Short- and long-term immune simulations of the designed construct demonstrated its potential as a potent immunogen, particularly in inducing Th1-type immunity, Th cell memory responses, and IgM production, which are key components of protective immunity against brucellosis, highlighting its promise for further experimental validation.

Materials and methods

Retrieval of FrpB Protein Sequences and In Silico Analysis

The TonB-dependent receptor domain-containing protein FrpB was selected as the target antigen for comparative sequence analysis. Protein sequence data were retrieved from the NCBI Identical Protein Groups database using the IPG accession WP_004681095.1 as the reference query, and sequence similarity was verified through direct comparison of identical protein group entries. A comprehensive in silico characterization was subsequently performed on the retrieved amino acid sequence. Signal peptide prediction was carried out with SignalP 6.0 (https://services.healthtech.dtu.dk/services/SignalP-6.0/) [27]. Virulence potential was assessed using VirulentHunter (http://www.unimd.org/VirulentHunter) [28] and VirulentPred (https://bioinfo.icgeb.res.in/virulent/) [29]. Subcellular localization was predicted with CELLO v2.5 (https://cello.life.nctu.edu.tw/) [30] and DeepLocPro 1.0

 doi:10.20944/preprints202512.0403.v1

(https://services.healthtech.dtu.dk/services/DeepLocPro-1.0/) [31], while membrane topology was evaluated using the TOPCONS webserver (https://topcons.cbr.su.se/pred/) [32].

Epitope Selection

Epitopes were predicted using the Next-Generation Immune Epitope Database (IEDB) tools (https://nextgen-tools.iedb.org/all-tools-list). B cell epitopes were predicted by the Bepipred Linear Epitope Prediction web server (https://tools.iedb.org/bcell/) at a threshold of 0.50. NetMHCpan EL 4.1 tool (IEDB recommended epitope predictor 2023.09) that predicts elution of peptides from MHC molecules using artificial neural networks (ANNs) was used for prediction of both MHCI and MHCII epitopes [33,34]. The method is trained on a combination of more than 850,000 quantitative Binding Affinity (BA) and Mass-Spectrometry Eluted Ligands (EL) peptides. Using the Allele Finder, a panel of 27 alleles each for MHCI (HLA-A and HLA-B) and MHCII were selected and used as a reference for epitope prediction. This panel provides >97% global population coverage for MHC class I and >99% coverage for MHC class II molecules across diverse ethnicities worldwide [35]. For epitope selection, the IEDB-recommended percentile rank thresholds were applied, using a cutoff of ≤1% for MHC class I and ≤10% for MHC class II to prioritize peptides with stronger predicted binding [36,37].

Antigenicity and Toxicity Prediction and Conservancy Analysis

The antigenicity of the predicted epitopes was determined by the Vaxijen v2.0 server (http://www.ddg-pharmfac.net/vaxijen/VaxiJen/VaxiJen.html) [38] using a threshold of 0.40. Epitopes predicted to be protective antigens were then scanned by the ToxinPred web server (https://webs.iiitd.edu.in/raghava/toxinpred/protein.php) for toxicity prediction using SVM (Swiss-Prot) based prediction method [39]. Moreover, epitope sequence conservancy was assessed using the IEDB Epitope Conservancy Analysis tool (**https://tools.iedb.org/conservancy/**) [40]. This tool calculates the degree of conservancy of an epitope within a given protein sequence set at different degrees of sequence identity. The degree of conservation is defined as the fraction of protein sequences containing the epitope at a given identity level [40].

In Silico Interferon Gamma Epitope Screening

Interferon gamma (IFN-γ) is a pivotal cytokine mediating protective immunity against brucellosis [41]. Therefore, antigenic non-toxic MHCI and MHCII binding epitopes were evaluated for their capacity to induce IFN-γ production using the IFNepitope2 server (https://webs.iiitd.edu.in/raghava/ifnepitope2/predict_human.php) [42]. This server utilizes composition-based algorithms to predict whether a given peptide is likely to be an IFN-γ inducer or non-inducer. Epitopes predicted to induce IFN-γ were selected based on a probability threshold of 0.47, set by the default dual peptide composition (DPC) based ET-model [42].

Population Coverage Analysis

Given the extensive polymorphism of human MHC (HLA) genes, with thousands of allelic variants described and each T cell epitope capable of eliciting responses only in individuals expressing compatible MHC molecules [43], evaluating HLA coverage is critical for rational vaccine design. In this study, the global population coverage of the predicted MHCI and MHCII epitopes was estimated using the IEDB Population Coverage tool (**http://tools.iedb.org/population/**) [43]. Coverage was calculated separately for class I and class II epitope sets, and then in combination, to estimate the proportion of the world population predicted to mount an immune response to the multi-epitope vaccine construct. Population coverage analyses were performed globally and for regions where brucellosis is endemic, with particular focus on North Africa, China, and India [44], to ensure that the selected epitopes provide broad HLA representation in high-burden areas.

 doi:10.20944/preprints202512.0403.v1

Epitope-Receptor Docking Analysis, Structure Assessment, and Binding Affinity

3D structures of the B cell epitopes and MHC class II epitopes were generated using the PEP-FOLD3 server (**https://mobyle.rpbs.univ-paris-diderot.fr/cgi-bin/portal.py#forms::PEP-FOLD3**), a computational tool designed for de novo prediction of peptide structures from amino acid sequences [45]. Molecular docking analyses using the ClusPro server were performed to evaluate the interactions of the epitopes with their corresponding receptors [46]. Crystal structure of the human B-cell antigen receptor of the IgM isotype (PDB code 7XQ8) [47] was retrieved from the Protein Data Bank for docking against the B cell epitopes. For docking MHC class II epitopes, crystal structures of the MHC II alleles HLA-DRA, DRB3*0101 (PDB code 2Q6W*)* [48] and HLA-DRB1*04:01 (PDB code 5JLZ) [49] were used. The top-ranked ClusPro model, defined by the largest cluster size, was retrieved and further assessed for structural quality using the Swiss Model structure assessment web server tool (**https://swissmodel.expasy.org/assess**) [50] and evaluated for binding affinity using the PRODIGY web server (**https://rascar.science.uu.nl/prodigy/**) [51], both established tools for structure validation and interaction energy prediction. ClusPro-generated 3D structures were visualized and analyzed using iCn3D, a web-based 3D molecular interactive structural analysis tool (https://www.ncbi.nlm.nih.gov/Structure/icn3d/) [52,53].

Construction of the Multiepitope Vaccine Construct

The final design of the multiepitope vaccine, Mvax, included 2 B cell, 2 MHC class I, and 3 MHC class II epitopes, which were strategically linked using a combination of flexible and rigid linkers including EAAAK, KK, AAY, and GPGPG. These linkers play critical roles in maintaining individual epitope immunogenicity and structural stability by preventing the formation of junctional epitopes and ensuring proper epitope processing [54–56]. To enhance the overall immunogenicity of the vaccine, human beta-defensin-3, a well-characterized antimicrobial peptide with immune-stimulatory properties, was fused to the N-terminus of the construct via an EAAAK linker, serving as a natural adjuvant to stimulate immune responses [57].

Secondary and 3D Structure Prediction and Validation

Prediction of secondary structure of the vaccines was performed using SOPMA protein secondary structure prediction server (https://npsa.lyon.inserm.fr/cgi-bin/npsa_automat.pl?page=/NPSA/npsa_sopma.html) [58,59], which employs the Self-Optimized Prediction Method with Alignment to classify amino acid residues into secondary structure states such as alpha-helix, beta-sheet, turns, and coils. The trRosetta webserver (https://yanglab.qd.sdu.edu.cn/trRosetta/) [60] were used to generate 3D structure models for Mvax and FrpB. trRosetta predicts the protein structure based on direct energy minimizations with a restrained Rosetta [60]. The top-ranked model from trRosetta was further validated for structural quality using the ProSA-web server (https://prosa.services.came.sbg.ac.at/prosa.php) [61], which assesses overall model quality and potential errors. Subsequently, this model underwent refinement via the GalaxyWeb refine server (https://galaxy.seoklab.org/cgi-bin/submit.cgi?type=REFINE) [62]. Model quality and stereochemical validity of refined 3D structure were assessed using the Errat tool and Ramachandran plot analysis through PROCHECK, both accessible via the Protein Structure Analysis and Verification Server, SAVES v6.1 (https://saves.mbi.ucla.edu/) [63].

Physicochemical Properties and Prediction of Discontinuous B-Cell Epitopes

The physicochemical properties of the vaccine candidates, including instability index, GRAVY index, and estimated half-life, were predicted using the Expasy ProtParam tool (https://web.expasy.org/protparam/) [64]. Antigenicity was evaluated via the VaxiJen server [38], while allergenicity was assessed using the AllerCatPro 2.0 web server (https://allercatpro.bii.a-star.edu.sg/) [65]. Solubility predictions of the constructs were carried out with the Protein-Sol server (https://protein-sol.manchester.ac.uk/) [66].

 doi:10.20944/preprints202512.0403.v1

Discontinuous B-cell epitopes were predicted using the IEDB ElliPro server (http://tools.iedb.org/ellipro/) [67]. The vaccine's 3D structure in PDB format was analyzed by ElliPro with default parameters, including a minimum score of 0.5 and a maximum distance of 6 angstrom.

Vaccine-Immune Receptor Docking Analysis

Molecular docking analyses were conducted using the ClusPro server [46] to simulate binding interactions between the vaccine constructs, Mvax and FrpB, and key human immune receptors. The selected receptors included the crystal structures of the human TLR4-MD2 complex (PDB code 3FXI) [68], TLR2/TLR6 complex (PDB code 3A79) [69] and the human B-cell antigen receptor of the IgM isotype (PDB code 7XQ8) [47]. TLR4 and TLR2/TLR6 were chosen for their critical role in innate immune recognition of Gram-negative bacteria like *Brucella* by detecting pathogen-associated molecular patterns (PAMPs) and initiating proinflammatory responses essential for protective immunity [70]. The pivotal role of vaccine-induced IgM antibodies in preventing early dissemination of *Brucella* by activating complement and restricting intracellular growth [26] underscores the importance of targeting IgM receptors in vaccine design for harnessing early immune defense. The ClusPro top-ranked docked complexes were validated with the PRODIGY web server to estimate binding affinity as noted earlier [51].

Immune Simulation Kinetics

The C-IMMSIM webserver (https://kraken.iac.rm.cnr.it/C-IMMSIM/index.php?page=1), which integrates position-specific scoring matrix (PSSM) and machine learning algorithms [71,72], was employed to simulate the human immune response to the vaccine candidates Mvax and FrpB. Simulation parameters were set as follows: simulation volume = 10, total simulation steps = 300 and 3285 to capture early and long-term immune responses; a single vaccine injection without lipopolysaccharide (LPS); adjuvant quantity set to 100; and antigen quantity set to 1000. For the human leukocyte antigen (HLA) allele panel, a cocktail comprising HLA-A*01:01, HLA-A*11:01, HLA-B*15:01, HLA-B*58:01, HLA-DRB3*01:01, and HLA-DRB4*01:01.

Results

Brucella FrpB: A Promising Vaccine Candidate with Multiple Key Attributes

Analysis of the TonB-dependent receptor domain-containing protein FrpB revealed 980 assembly accessions across diverse *Brucella* species, including *B. melitensis*, *B. abortus*, and *B. suis*. NCBI protein database analysis conducted in this study showed that the FrpB protein exhibited 100% sequence identity among all retrieved *Brucella* accessions (Supplementary Spreadsheet S1). This conservation positions FrpB as an attractive vaccine target for developing broadly protective vaccines against diverse *Brucella* pathogens responsible for human brucellosis. Moreover, as shown in Figure 1, in silico analyses predict that FrpB possesses multiple other features favorable for a vaccine candidate. SignalP6 identified a classical Sec/SPI signal peptide with a predicted cleavage site between positions 23 and 24 and a high confidence score of 0.999. TOPCONS topology analysis further confirmed a 23-residue signal peptide, with the remaining 638 residues located outside, indicating that most of the protein is likely accessible to the host immune system. Subcellular localization tools CELLO v.2.5 and DeepLocPro-1.0 also classified FrpB as an outer membrane protein, with high prediction scores of 4.65 and 1.0, respectively. Analysis with the VirulentPred server yielded a virulence score of 1.02, whereas VirulenceHunter produced a score of 0.96 and additionally predicted functional roles in immune modulation with a score of 0.988, adherence with a score of 0.486, and nutritional/metabolic processes with a score of 1.0. Employing the Vaxign2 server [73] further confirmed the uniqueness of FrpB, revealing no human or animal homologs and an adhesion function probability of 0.52, consistent with VirulenceHunter predictions.

 doi:10.20944/preprints202512.0403.v1

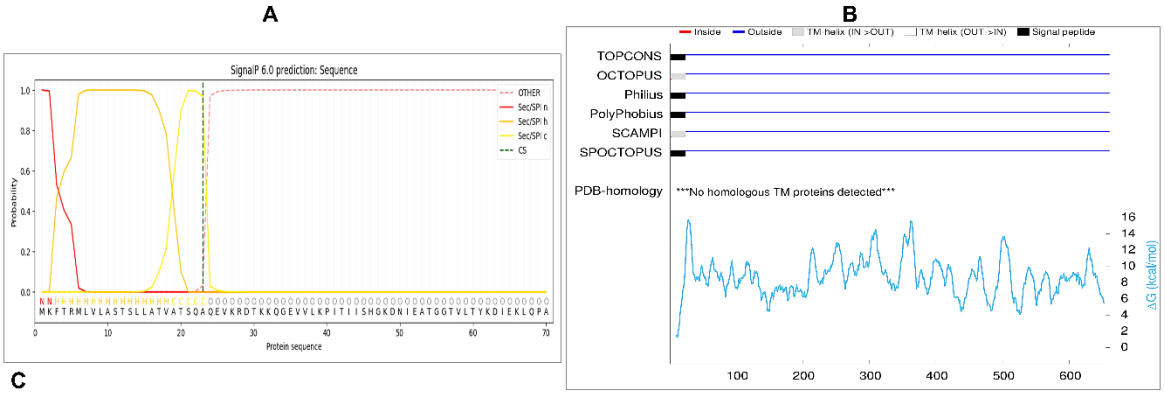

C

Server name	Description	Score	Result
SignalP6.0	Predictor of the presence of signal peptides	0.999	Signal peptide (Sec/SPI)
VirulentHunter	Predictor of virulent proteins	0.96	Virulent
VirulentPred	Predictor of virulent proteins	1.02	Virulent
CELLO v.2.5	Predictor of subcelllular localization	4.65	Outer membrane
DeepLocPro - 1.0	Predictor of subcellular localization	1	Outer membrane

Figure 1. Comprehensive in silico analysis of *Brucella* FrpB. A. SignalP 6.0 webserver prediction showing the presence of a 23-signal peptide sequence in FrpB. **B.** TOPCONS webserver analysis of the FrpB sequence depicting its predicted topology. **C.** Summary of in silico analysis outputs for FrpB obtained from multiple prediction servers showing predicted virulence and localization. Note: Citations for all computational servers utilized are included in the Materials and Methods section.

Previous studies have identified FrpB as an iron-regulated outer membrane protein involved in maintaining cell envelope integrity and contributing to *Brucella* virulence [74]. It has also been detected in outer membrane vesicles and suggested to play roles in immune modulation and bacterial survival within the host [75]. Moreover, FrpB-based vaccination has been shown to elicit Th1 cell immune responses and confer protection against *B. melitensis* and *B. abortus* challenge in mice [76].

Together, these predictions and published findings support FrpB as a strong antigenic target for antivirulence vaccine development against *Brucella* infection.

Selected B- and T-Cell Epitopes

Following assessment of different FrpB's properties, in this study, B cell and T cell epitopes were predicted using the IEDB resource to identify FrpB's peptide sequences recognizable by the human immune system. The epitopes were predicted using cutoff values of 0.350 for B cell epitopes, ≤1% percentile rank for MHC class I, and ≤10% percentile rank for MHC class II to prioritize peptides with stronger predicted binding affinity [36,37]. As shown in Table 1, a final list of epitopes was selected based on their high prediction scores, including 2 B cell epitopes (16-mer at residue positions 179-194 and 21-mer at positions 209-229), 2 MHC class I epitopes (9-mer at positions 412-420 and 53-61), and 3 MHC class II epitopes (each 15-mer at 23-37, 278-292, and 303-317). The selected epitopes exhibited no toxicity and displayed antigenic scores ranging from 0.77 to 1.16, indicating strong potential as protective antigens. Using the IFNepitope2 webserver, both the MHCI and MHCII epitopes were identified as interferon-gamma inducers with scores ranging from 0.5 to 0.82. Sequence analysis revealed that all selected epitopes were 100% conserved across the retrieved *Brucella* FrpB sequences (Supplementary Spreadsheet S1, n= 980 assembly accessions) available in the NCBI Protein Database.

Table 1. Summary of candidate epitopes selected for this study.

 doi:10.20944/preprints202512.0403.v1

Residue position (start-end)	Epitope Sequence	Epitope type	Conservancy %	Vaxijen score	IFNepitope2 score	Toxicity
179-194	YGTNGRGFSGSTAAYG	B-cell	100	1.54	-	Non-Toxin
209-229	SGHNYKNGDGTEILGTEPAAR	B-cell	100	1.61	-	Non-Toxin
412-420	ASVNGTLSY	MHCI	100	1.08	0.64	Non-Toxin
53-61	ATGGTVLTY	MHCI	100	1.12	0.82	Non-Toxin
23-37	AQEVKRDTKKQGEVV	MHCII	100	1.11	0.57	Non-Toxin
278-292	DSVNIKYTRTDATDM	MHCII	100	1.31	0.5	Non-Toxin
303-317	RNDYWRNDYQNRTNG	MHCII	100	0.77	0.52	Non-Toxin

High Population Coverage of Selected T-Cell Epitopes in Brucellosis-Endemic Regions

The shortlisted epitopes and their corresponding HLA alleles (Table 2) were subjected to population coverage analysis using the IEDB tool [43].

Table 2. Predicted binding human alleles for the candidate epitopes.

Epitope Sequence	Predicted binding alleles
ASVNGTLSY	HLA-A*30:02, HLA-B*15:01, HLA-A*01:01, HLA-A*26:01, HLA-A*11:01, HLA-B*58:01, HLA-B*35:01, HLA-A*32:01, HLA-B*57:01, HLA-A*03:01
ATGGTVLTY	HLA-A*30:02, HLA-A*01:01, HLA-A*11:01, HLA-A*32:01, HLA-B*15:01, HLA-A*26:01, HLA-B*58:01, HLA-A*03:01, HLA-B*57:01, HLA-B*35:01
AQEVKRDTKKQGEVV	HLA-DRB1*03:01, HLA-DRB1*13:02, HLA-DRB1*11:01, HLA-DRB1*08:02, HLA-DRB3*01:01
DSVNIKYTRTDATDM	HLA-DRB4*01:01, HLA-DRB1*04:01, HLA-DRB1*07:01, HLA-DQA1*04:01, HLA-DQB1*04:02, HLA-DRB1*09:01, HLA-DRB1*04:05, HLA-DRB1*08:02, HLA-DQA1*05:01, HLA-DQB1*02:01, HLA-DQA1*03:01, HLA-DQB1*03:02
RNDYWRNDYQNRTNG	HLA-DRB3*01:01, HLA-DRB3*02:02, HLA-DRB1*03:01, HLA-DRB1*13:02, HLA-DPA1*01:03, HLA-DPB1*02:01, HLA-DRB1*04:01, HLA-DPB1*04:01

Analyses were performed globally and for brucellosis-endemic regions, with particular focus on North Africa, China, and India [44], to ensure broad HLA representation in high-burden areas. Coverage was calculated separately for MHC class I and class II epitope sets, and in combination, to estimate the proportion of the world population predicted to respond to the multi-epitope vaccine construct. As shown in Figure 2, the MHC class I epitopes achieved 64.93% global population coverage, whereas class II epitopes reached 98.82%, with class I and class II combined covering 99.59% worldwide. Coverage in selected endemic regions was similarly high for class I, class II, and the combined classes: 52.64%, 97.68%, and 98.90% in North Africa; 58.02%, 99.50%, and 99.79% in India; and 64.95%, 97.52%, and 99.13% in China, respectively (Figure 2). As shown in Supplementary Spreadsheet S2, the analysis also showed that the vaccine has 100% class-combined coverage in the USA, Mexico, Brazil, Venezuela, and Sweden. These results demonstrate excellent population coverage, supporting the vaccine construct's potential for broad protective efficacy worldwide and in brucellosis-endemic areas.

 doi:10.20944/preprints202512.0403.v1

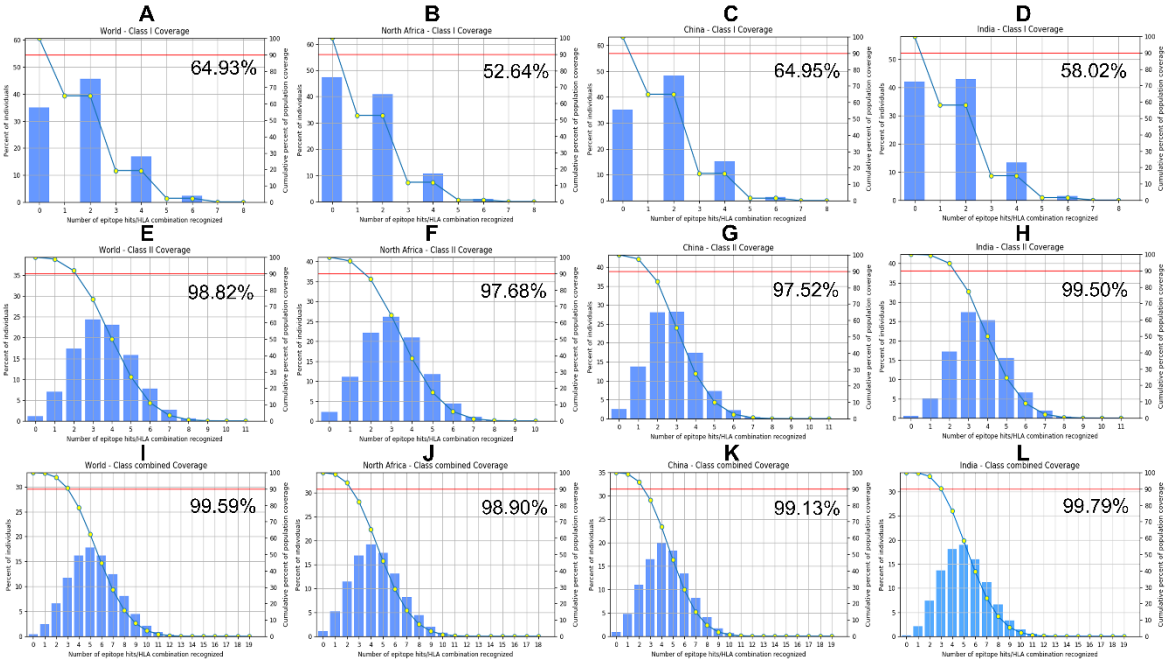

Figure 2. Population coverage of selected epitopes worldwide and in selected *Brucella*-endemic regions. **A-D**. Population coverage of selected MHCI epitopes across the world (A), North Africa (B), China (C), and India (D). **E-H.** Population coverage of selected MHCII epitopes across the world (E), North Africa (F), China (G), and India (H). **I–L.** Population coverage of combined MHCI and MHCII epitopes across the world (I), North Africa (J), China (K), and India (L). Population coverage analysis was performed using the IEDB resource.

Selected B- and T-Cell Epitopes Exhibit High Binding Affinity to Human Receptors

Following confirmation of broad T-cell epitope population coverage, B-cell and MHC class II epitopes were evaluated for binding to human receptors using ClusPro docking [46]. As revealed in Table 3, docking the B-cell epitope YGTNGRGFSGSTAAYG to the human IgM B-cell antigen receptor crystal structure (PDB: 7XQ8) yielded a top cluster with 333 members, while the epitope SGHNYKNGDGTEILGTEPAAR produced a cluster of 308 members with the same receptor. For MHC class II epitopes, docking AQEVKRDTKKQGEVV to HLA-DRB1*01:01 (PDB: 2Q6W) generated a cluster of 292 members, and docking RNDYWRNDYQNRTNG to the same allele resulted in 282 members. Finally, docking DSVNIKYTRTDATDM to HLA-DRB1*04:01 (PDB: 5JLZ) yielded 171 members. Although ClusPro reported highly negative PIPER docking scores for all top-ranked models in this study, PIPER energy does not represent actual binding free energy and should not be used for model ranking [46]. Therefore, evaluation of ClusPro docking output in this study relied solely on cluster population size rather than energy scores, as recommended [46]. Larger cluster sizes suggest more stable and reliable docking conformations.

Table 3. Structure assessment and binding affinity of epitope-receptor complexes.

Ligand	Human receptor		Top Model ClusPro cluster size	SWISS-MODEL structure assessment				PRODIGY binding affinity	
	Description	PDB code		MolProbity Score	Ramachandran favored	Ramachandran outliers	QMEANDisCo Global	ΔG (kcal mol^{-1})	K_d (M) at 37 ℃
YGTNGRGFSGSTAAYG	Crystal structure of human B-cell antigen receptor of the IgM isotype	7XQ8	333	3.20	92.76%	0.58%	0.71±0.05	-11.6	6.5×10^{-9}

 doi:10.20944/preprints202512.0403.v1

SGHNYKNGDG TEILGTEPAAR	Crystal structure of human B-cell antigen receptor of the IgM isotype	7XQ8	308	3.20	92.62%	0.74%	0.70±0.05	-8.1	2×10^{-6}
AQEVKRDTKK QGEVV	Crystal structure of MHCII allele HLA-DRA, DRB3*0101	2Q6W	292	2.97	93.68%	0.66%	0.83±0.05	-13.0	6.7×10^{-10}
DSVNIKYTRTD ATDM	Crystal structure of MHCII allele HLA-DRB1*04:01	5JLZ	171	2.35	96.60%	0.39%	0.86±0.05	-11.0	1.8×10^{-8}
RNDYWRNDY QNRTNG	Crystal structure of MHCII allele HLA-DRA, DRB3*0101	2Q6W	282	2.95	93.95%	0.53%	0.83±0.05	-12.8	9.5×10^{-10}

However, for further in silico validation, the ClusPro- top-ranked models underwent structural validation using SWISS-MODEL and binding affinity prediction with the PRODIGY server, ensuring thorough evaluation of model stability and interaction strength (Table 3). These analyses yielded MolProbity scores of 2.35-3.20, Ramachandran favored regions of 92.62-96.60%, Ramachandran outliers of 0.24-0.74%, QMEANDisCo global scores of 0.70±0.05 to 0.86±0.05, binding free energies (ΔG) of -8.1 to -13.0 kcal/mol, and dissociation constants (Kd) of 2×10^{-6} to 9.5×10^{-10} M at 37°C. These metrics confirm high-quality structures and strong predicted binding affinities, supporting the stability of the epitope-receptor interactions.

After confirming the binding affinities between the epitopes and their respective receptors, the top-ranked 3D docked complexes were visualized and analyzed using iCn3D, a web-based interactive tool for molecular structural analysis [52,53]. As shown in Figure 3, the B-cell- and MHC II-epitopes bind to spatially distinct sites on their respective immune receptors, indicating non-overlapping binding interfaces and suggesting that each epitope can independently engage its target receptor. This supports their compatibility within a multiepitope vaccine and suggests that the construct has the potential to elicit both humoral and $CD4^+$ T cell-mediated immune responses.

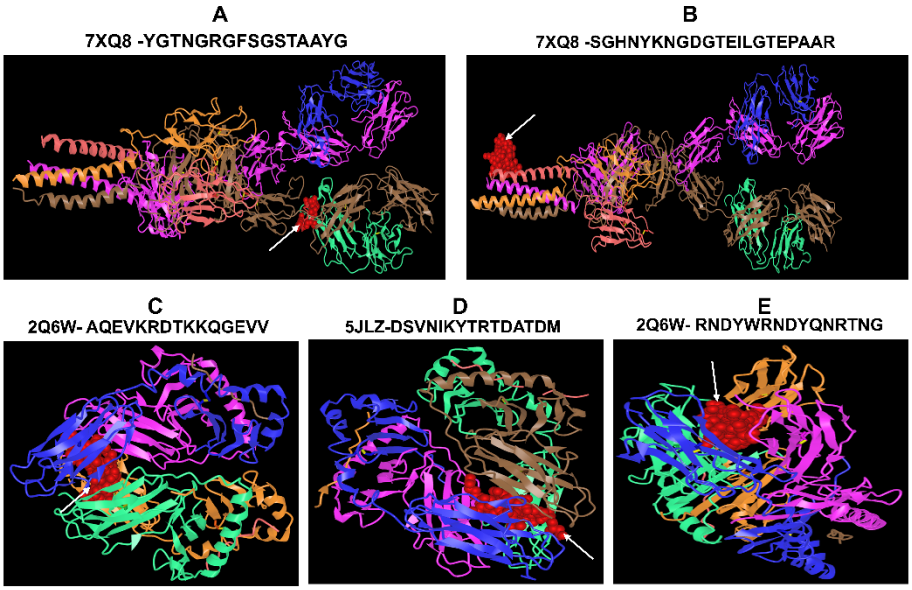

Figure 3. iCn3D visualization of molecular docking of selected B cell and MHCII epitopes with human immune receptors. Crystal structures were retrieved from the Protein Data Bank (https://www.rcsb.org/) prior to ClusPro docking. Epitope structures were generated by the PEP-FOLD3 server, and docking was performed

 doi:10.20944/preprints202512.0403.v1

against the retrieved PDB crystal structures. The resulting ClusPro-generated 3D complexes were visualized and analyzed using iCn3D, a web-based interactive tool for 3D molecular structural analysis. The receptors are displayed in ribbon style with distinct colors, while the epitopes are shown in red sphere style and indicated by white arrows. **A.** Docking B cell epitope YGTNGRGFSGSTAAYG to the crystal structure of the human B-cell antigen receptor IgM isotype (PDB code 7XQ8). **B.** Docking B cell epitope SGHNYKNGDGTEILGTEPAAR to the crystal structure of the human B-cell antigen receptor IgM isotype (PDB code 7XQ8). **C.** Docking MHCII epitope AQEVKRDTKKQGEVV to the crystal structure of the MHCII allele HLA-DRA/DRB3*0101 (PDB code 2Q6W). **D.** Docking MHCII epitope DSVNIKYTRTDATDM to the crystal structure of the MHCII allele HLA-DRB1*04:01 (PDB code 5JLZ). **E.** Docking of the MHCII epitope RNDYWRNDYQNRTNG to the crystal structure of the MHCII allele HLA-DRA/DRB3*0101 (PDB code 2Q6W).

Multi-Epitope Vaccine Assembly from Diverse Epitopes

The selected epitopes from the FrpB sequence (Figure 4A) were assembled into a multi-epitope vaccine construct (Mvax) using optimized linkers to enhance immunogenicity and processing (Figure 4B). Two B cell epitopes were joined by a KK linker, which minimizes junctional neoepitope formation, prevents unwanted antibody responses at linker junctions, and serves as cleavage sites for cathepsin B to facilitate MHC class II antigen presentation [77,78]. Two MHCI epitopes were connected via an AAY linker, which acts as specific proteasome cleavage sites to generate mature MHC class I epitopes and promote cytotoxic T cell responses [79,80]. Three MHCII epitopes were linked with GPGPG linkers to promote helper T cell responses while avoiding junctional epitopes that could compromise vaccine efficacy [78]. A rigid α-helical EAAAK linker was employed to separate epitope types and the B cell epitopes from the adjuvant, preserving domain functionality and enhancing overall protein stability [78]. Human β-defensin 3 was incorporated as an in-built adjuvant due to its established immunostimulatory properties that amplify both innate and adaptive immune responses [57].

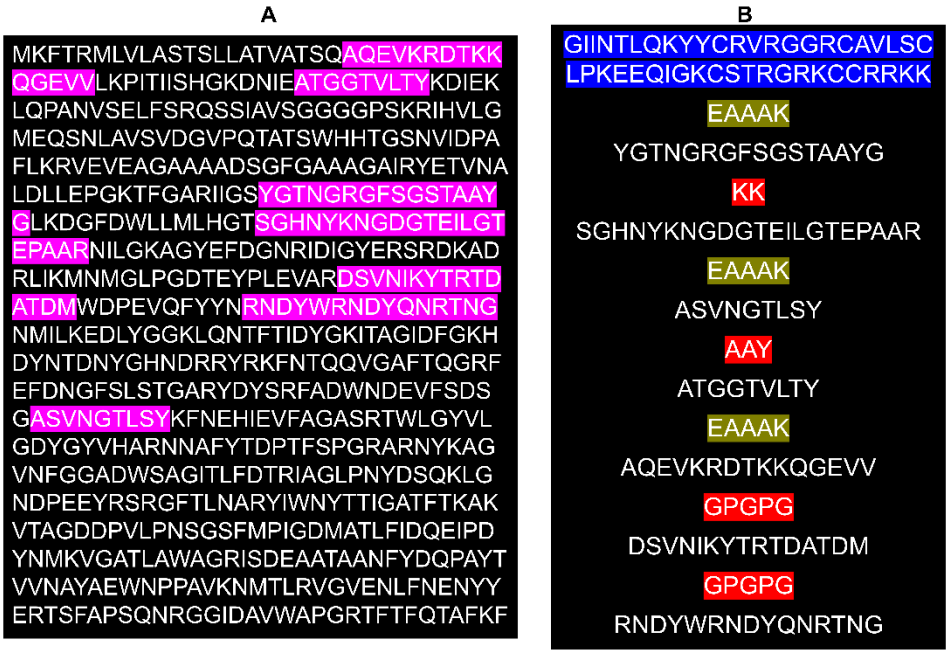

Figure 4. Schematic representation of the final assembled multiepitope vaccine construct. A. Amino acid sequence of the native FrpB protein (accession WP_004681095.1). **B.** Sequence of the 175-mer multiepitope vaccine construct (Mvax) containing seven epitopes connected by different linkers. The rigid linker **EAAAK** separates different types of epitopes and links the Beta defensin (positions 1-45) at the N-terminus of the assembled epitopes. **KK** linkers connect the two B cell epitopes, **AAY** linkers connect the MHCI epitopes, and **GPGPG** linkers connect the MHCII epitopes.

 doi:10.20944/preprints202512.0403.v1

Mvax Demonstrates Superior Physicochemical Properties

Mvax is only 175 amino acids long, substantially shorter than the 661-residue native FrpB protein, which may facilitate easier production and purification. Additionally, in silico analyses demonstrate that Mvax possesses superior physicochemical properties compared to native FrpB, as detailed in Table 4. The molecular weight of FrpB is 72,932.84 Da, whereas Mvax is substantially lighter at 18,701.86 Da. Solubility is another key improvement: FrpB has a low scaled solubility (QuerySol) of 0.275, below the population average solubility (PopAvrSol = 0.45) for soluble *E. coli* proteins [66], while Mvax exhibits a much higher QuerySol of 0.808, indicating that Mvax is better suited for efficient expression and downstream handling. Antigenicity analysis revealed that the FrpB scored 0.602, while Mvax achieved a higher score of 1.06, indicating greater antigenic potential. Overall, these results demonstrate that Mvax has enhanced physicochemical properties, potentially supporting its suitability as a stable and effective vaccine candidate.

Table 4. Physicochemical properties of the designed vaccine construct.

Predicted score	FrpB	MAvax
Molecular weight	72932.84	18701.86
Theoretical pI	5.71	9.63
Instability index	31.12	27.86
Aliphatic index	66.19	49.20
GRAVY index	-0.486	-0.881
Scaled solubility score	0.275	0.808
Vaxijen score	0.602	1.06
Allergenicity	Non-allergenic	Non-allergenic
Estimated half-life	30 hours (mammalian reticulocytes, in vitro). >20 hours (yeast, in vivo). >10 hours (*Escherichia coli*, in vivo)	30 hours (mammalian reticulocytes, in vitro). >20 hours (yeast, in vivo). >10 hours (*Escherichia coli*, in vivo)

Structural Modeling and Validation of Mvax Crystal Structure

As presented in Figure 5A, the SOPMA secondary structure analysis indicates Mvax is predominantly flexible, with random coil comprising 98 residues (56%), followed by extended strands with 39 residues (22.29%) and alpha helices with 38 residues (21.71%). This distribution suggests a mixed secondary structure with substantial coil content that may favor epitope exposure and immune recognition. The 3D structure of Mvax was initially constructed using trRosetta, yielding a top model with an estimated TM-score of 0.335, indicating a moderate-confidence global fold. This model was subsequently refined with the GalaxyWeb server, which generated five candidate structures, from which the best-scoring model was selected for further analysis. The refined 3D model of Mvax (Figure 5B) was found to have a ProSA-web Z-score of -4.95 (Figure 5C). Further structural validation using SAVES server showed an overall model quality of 94.87% (Figure 5D). Ramachandran plot analysis by PROCHECK confirmed model stereochemical quality, with 97.9% of residues in allowed regions (91.7% most favored, 5.6% additional allowed, 0.7% generously allowed) and only 2.1% in disallowed regions (Figure 5E). Swiss-Model assessment tool further verified 0.58% Ramachandran outliers and 0% rotamer outliers. Together, these metrics affirm the structural reliability and correctness of the modeled protein geometry for downstream use and analysis.

 doi:10.20944/preprints202512.0403.v1

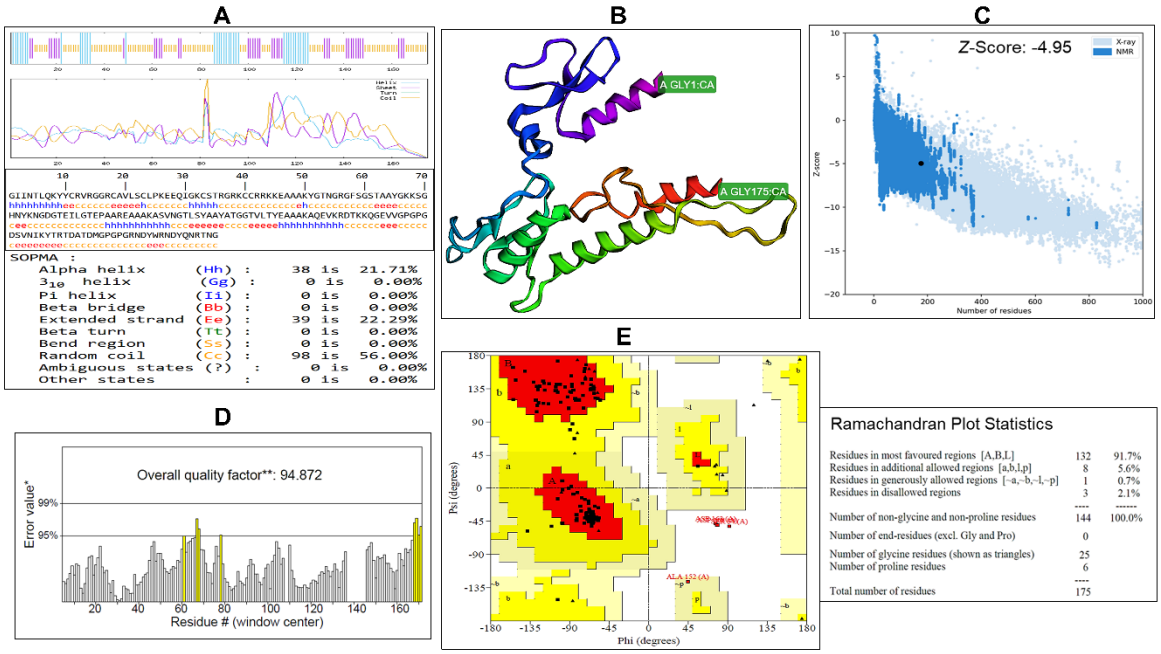

Figure 5. Predicted secondary and tertiary structures of the designed multiepitope vaccine construct. A. Secondary structure model predicted and analyzed using the SOPMA server. **B.** 3D structure of the designed vaccine generated by trRosetta and refined using the GalaxyWeb server. **C.** Structural validation of the refined model using ProSA-web. **D.** Structural quality assessment using SAVES v6.1. **E.** Ramachandran plot and statistics generated by SAVES v6.1 to evaluate stereochemical quality.

ElliPro Analysis Identifies Multiple High-Scoring Conformational Epitopes

The refined 3D structure of Mvax was analyzed by Ellipro server for presence of conformational epitopes [67]. Analysis at a threshold of 0.50 predicted 4 conformational B-cell epitopes with lengths of 19, 36, 29, and 5 amino acid residues and corresponding scores of 0.83, 0.734, 0.67, and 0.614, respectively (Figure 6A-E). The presence of multiple conformational epitopes highlights the vaccine construct's potential to stimulate humoral immune responses [81].

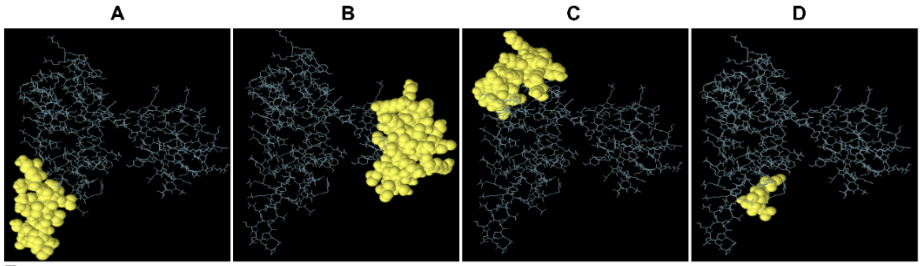

E

Number	Residues	Number of residues	ElliPro score
A	A:D127, A:K130, A:Q131, A:G132, A:E133, A:V134, A:V135, A:G136, A:P137, A:G138, A:P139, A:G140, A:D141, A:S142, A:V143, A:N144, A:I145, A:K146, A:Y147	19	0.83
B	A:G1, A:I2, A:I3, A:N4, A:T5, A:L6, A:Q7, A:K8, A:R12, A:G16, A:R17, A:C18, A:A19, A:V20, A:L21, A:S22, A:C23, A:L24, A:P25, A:K26, A:E27, A:E28, A:Q29, A:G31, A:K32, A:C33, A:S34, A:T35, A:R36, A:G37, A:R38, A:K39, A:C40, A:C41, A:R43, A:K44	36	0.734
C	A:S59, A:G60, A:S61, A:T62, A:A63, A:A64, A:Y65, A:G66, A:K67, A:K68, A:S69, A:G70, A:H71, A:G83, A:T84, A:E85, A:P86, A:A87, A:R89, A:E90, A:A105, A:Y106, A:A107, A:T108, A:G109, A:G110, A:T111, A:V112, A:L113	29	0.67
D	A:D168, A:N171, A:T173, A:N174, A:G175	5	0.614

Figure 6. Predicted discontinuous epitopes in the designed vaccine construct. **A-D.** 3D structure of Mvax showing different conformational epitopes arranged from high to low based on their ElliPro scores. **E.** Summary table of residues, positions, residue numbers, and scores for each predicted conformational epitope.

 doi:10.20944/preprints202512.0403.v1

Mvax Exhibits High Binding Affinity to Immune Receptors

In order to assess the binding interactions of Mvax with various immune receptors, protein-protein docking was performed using the ClusPro server [46]. Figure 7 shows the cluster sizes from ClusPro docking of Mvax with three receptors. The clusters have 52, 128, and 95 members for TLR4/MD2, TLR2/TLR6, and BCR-IgM, respectively. For comparison, the native FrpB protein was found to form smaller clusters of 32, 109, and 60 members with the same receptors. Larger ClusPro cluster sizes suggest a more stable native complex, occupying a well-defined energy well on the energy landscape [46]. To estimate binding free energy, PRODIGY was applied to the top-ranked ClusPro cluster for each complex. At 37°C, simulating human physiological temperature, PRODIGY predicted stronger binding affinities for Mvax to both TLRs compared with native FrpB. The TLR4/MD2-Mvax complex exhibited a ΔG of -22.6 kcal mol^{-1} with a Kd of 1.2×10^{-16} M (Figure 7A), whereas the TLR4/MD2-FrpB complex showed -18 kcal mol^{-1} and 1.7×10^{-13} M (Figure 7D). Similarly, the TLR2/TLR6-Mvax complex had a ΔG of -14 kcal mol^{-1} and a Kd of 3.4×10^{-11} M (Figure 7B), while the TLR2/TLR6-FrpB complex yielded -11.4 kcal mol^{-1} and 3.4×10^{-11} M (Figure 7E). In contrast, the IgM BCR-Mvax complex displayed a ΔG of -19.7 kcal mol^{-1} and a Kd of 1.3×10^{-14} M (Figure 7C), whereas the IgM BCR-FrpB complex showed a stronger predicted affinity of -23 kcal mol^{-1} and 5.1×10^{-17} M (Figure 7F). Overall, lower (more negative) ΔG and Kd values correspond to tighter binding [82]; however, the exceptionally strong predicted binding affinities observed in this study remain in silico estimates that indicate relative rather than absolute affinity and require further experimental validation. Comparable PRODIGY scores have been reported with other in silico designed vaccines [83].

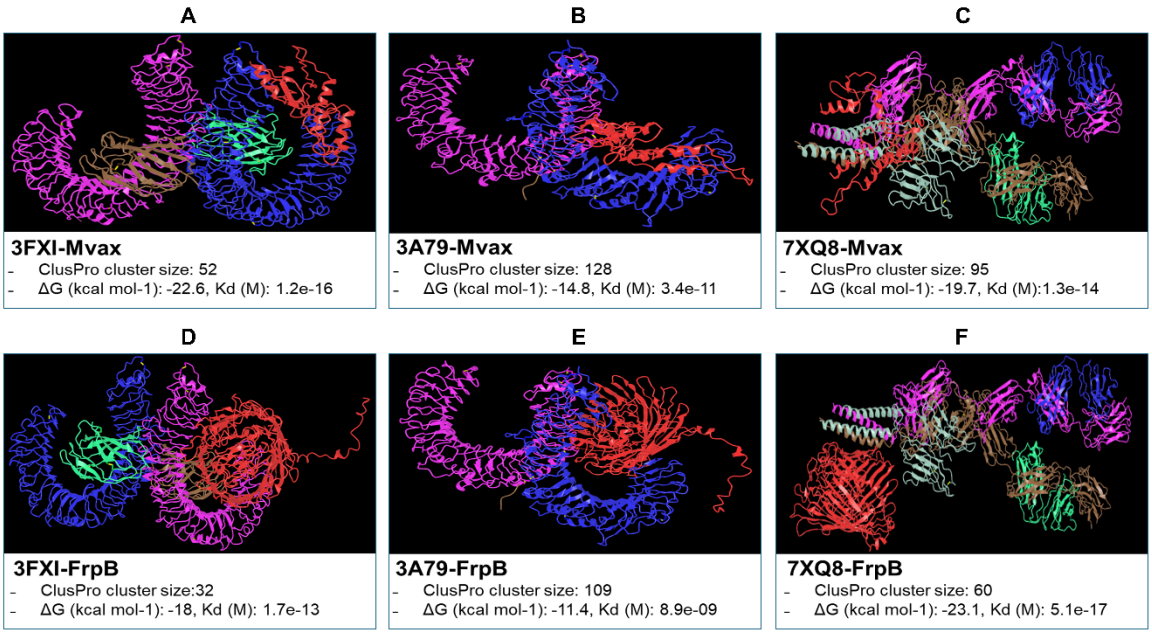

Figure 7. iCn3D visualization of molecular docking of Mvax and FrpB with human immune receptors. Crystal structures were retrieved from the Protein Data Bank (https://www.rcsb.org/) prior to ClusPro docking. ClusPro-generated 3D complexes were visualized and analyzed using iCn3D, a web-based interactive tool for 3D molecular structural analysis. The receptors are shown in ribbon style with distinct non-red colors, whereas the epitopes are highlighted in red ribbon style. Cluster sizes from ClusPro and PRODIGY-derived binding affinities (ΔG in kcal·mol^{-1} and Kd in M) for each docked complex are shown below each image. PRODIGY analysis was performed at 37 °C. **A.** Docking Mvax to the TLR4/MD2 complex (PDB code 3FXI). **B.** Docking Mvax to the TLR2/TLR6 complex (PDB code 3A79). **C.** Docking Mvax to the human B-cell antigen receptor IgM isotype (PDB 7XQ8). **D.** Docking FrpB to the TLR4/MD2 complex (PDB code 3FXI). **E.** Docking FrpB to the TLR2/TLR6 complex (PDB code 3A79). **F.** Docking FrpB to the human B-cell antigen receptor IgM isotype (PDB 7XQ8).

 doi:10.20944/preprints202512.0403.v1

Three-Year Modeling Highlights Mvax's Enhanced Th1 Memory Response

T-helper type 1 (Th1) cells and their cytokines (IL-12, IFN-γ, IL-2) play essential roles in the protective immune response against *Brucella* spp., driving macrophage activation and bacterial clearance [84,85]. In this study, a 100-day in silico simulation analysis following a single-dose injection demonstrated the overall superiority of Mvax in inducing T helper (Th) cell simulated responses (Figure 8). Specifically, Mvax elicited a strong Th1-type immune simulated response, with the Th1 cell population reaching approximately ~80,000 cells/mm³ (Figure 8A), compared with ~30,000 cells/mm³ induced by a single dose of FrpB (Figure 8C). Cytokine profiles revealed rapid simulated innate immune activation following vaccination for either vaccine candidates (Figure 8B and D). IL-12 levels peaked at 5 days post-vaccination, reaching ~ 25,000 ng/ml for Mvax (Figure 8B) and ~23,500 ng/ml for FrpB (Figure 8D). IL-2 surged concurrently, with Mvax inducing ~500,000 ng/ml (Figure 8B) compared with ~192,000 ng/ml for FrpB (Figure 8D). By day 12, interferon-gamma (IFN-γ) production reached its peak for both vaccines, with Mvax eliciting ~450,000 ng/ml (Figure 8B) versus ~412,000 ng/ml for FrpB (Figure 8D). Additionally, Mvax triggered higher simulated levels of TGF-β (~215,000 ng/ml versus ~65,000 ng/ml) and IL-10 (~65,000 ng/ml versus ~37,500 ng/ml), likely suggesting enhanced immunoregulatory responses to help prevent excessive inflammation.

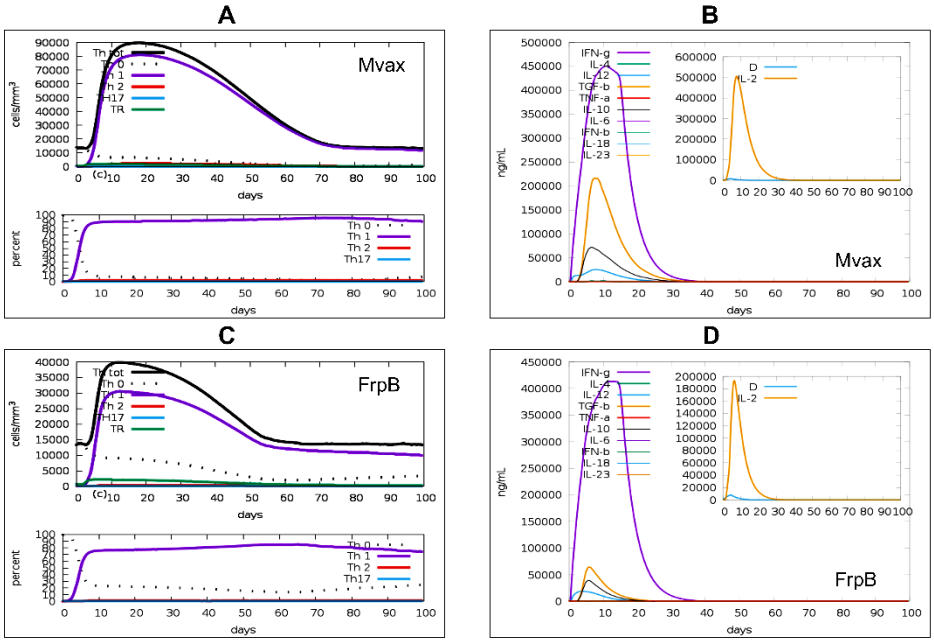

Figure 8. Predicted T helper cell responses and cytokine profiles following a single dose of Mvax or FrpB. C-ImmSim was used to simulate human immune responses to a single dose. Simulation parameters: simulation volume = 10; total steps = 300 (capturing early immune responses); single injection without LPS; adjuvant quantity = 100; antigen quantity = 1000. An HLA allele cocktail (HLA-A*01:01, HLA-A*11:01, HLA-B*15:01, HLA-B*58:01, HLA-DRB3*01:01, HLA-DRB4*01:01) was used. **A.** Predicted populations and percentages of T helper subsets in response to a single dose of Mvax. **B.** Simulated cytokine profiles induced by a single dose of Mvax. **C.** Predicted populations and percentages of T helper subsets in response to a single dose of FrpB. **D.** Simulated cytokine profiles induced by a single dose of FrpB.

As revealed in Figure 9, analysis at 20 days post-vaccination further demonstrated Mvax's superiority in simulated memory induction, generating approximately ~3.4-fold more memory T helper (Th) cells per mm³ (~925 cells/mm³ for Mvax ((Figure 9A)) versus ~275 cells/mm³ for FrpB (Figure 9B)). Given the importance of durable memory T cell responses for long-term vaccine efficacy, a 3-year in silico simulation was conducted to assess sustained cellular immunity. Interesting, simulated memory responses persisted after a single dose of either vaccine; however, at day 1095 (~3

 doi:10.20944/preprints202512.0403.v1

years), as shown in Figure 9C, Mvax maintained roughly double the memory Th cell count (~50 cells/mm³) compared with FrpB (~25 cells/mm³) (Figure 9D). This enhanced persistence, combined with Mvax's superior early cytokine induction and memory cell generation, highlights its potential to elicit robust Th1 immunity against *Brucella*.

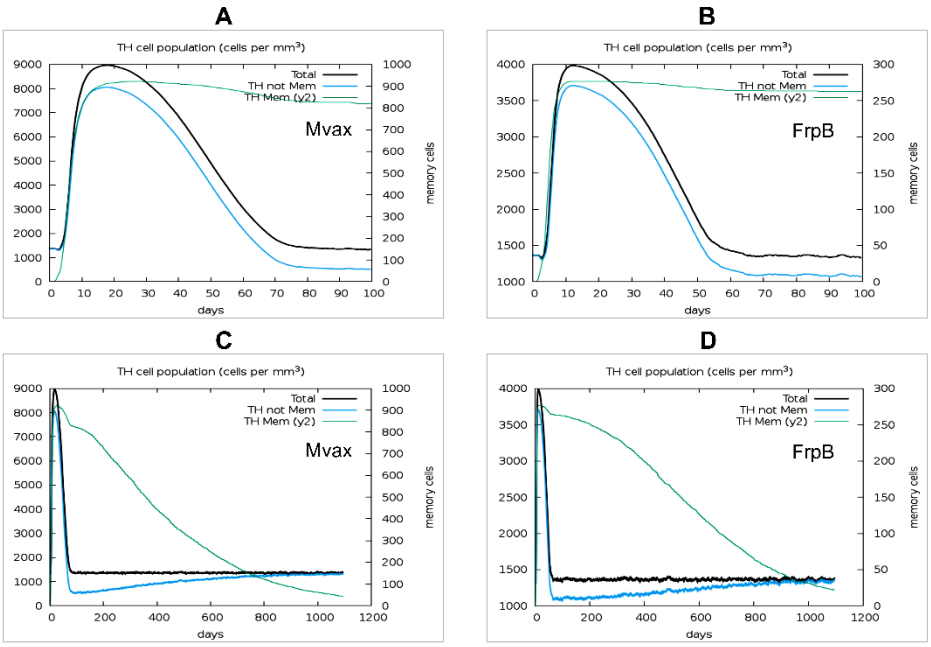

Figure 9. Predicted long-term immunological memory simulation following a single dose of Mvax or FrpB. Simulations were conducted using the same parameters as in Figure 8, with the number of simulation steps extending to 3285 to model immune responses over a 3-year period. A single-dose regimen was applied. Predicted T helper (Th) cell populations are shown for Mvax during the 100-day simulation period **(A)**, FrpB during the 100-day simulation period **(B)**, Mvax during the 3-year simulation period **(C)**, and FrpB during the 3-year simulation period **(D)**.

Simulation Demonstrates Mvax Enhances IgM Plasma Cells and IgM Antibody Levels

We recently demonstrated that secretory IgM elicited by S19 vaccination activates complement pathways to restrict *Brucella melitensis* dissemination during the first two weeks post-challenge in mice, as evidenced by significantly higher splenic bacterial burdens in sIgM-deficient animals [26]. This early humoral immunity complements T cell responses by restricting systemic bacterial spread before adaptive cellular immunity fully engages later on. These findings underscore the strategic importance of inducing IgM in multiepitope vaccines designed to emulate the effectiveness of live-attenuated vaccines like S19.

In the present study, as revealed in Figure 10, simulation analysis revealed that Mvax increased simulated plasma cells of all isotypes, with IgM-isotype plasma cells notably elevated by approximately 7.7-fold compared with FrpB, 30 cells/mm³ for Mvax (Figure 10A) versus ~3.9 cells/mm³ (Figure 10C). Correspondingly, simulated IgM antibody levels due to Mvax increased roughly 10-fold, ~40,000 ng/ml for Mvax (Figure 10B) versus ~4,000 ng/ml for FrpB.

Besides the predicted induction of interferon-gamma, IL-12, and IL-2 as noted earlier (Figure 8), elevated levels of antibodies IgG1, IgG2, and IgM following Mvax or FrpB stimulation further support a Th1-type immune response (Figure 10B and D). This aligns with the known role of Th1 cells in promoting IgM, IgG1, and IgG2 antibodies in humans [86].

Together with Mvax's predicted ability to elicit robust Th1 responses and durable memory T cell populations, these findings highlight its potential to stimulate both humoral and cellular immunity,

 doi:10.20944/preprints202512.0403.v1

positioning Mvax as a promising multiepitope vaccine candidate potentially capable of providing effective early protection against human brucellosis.

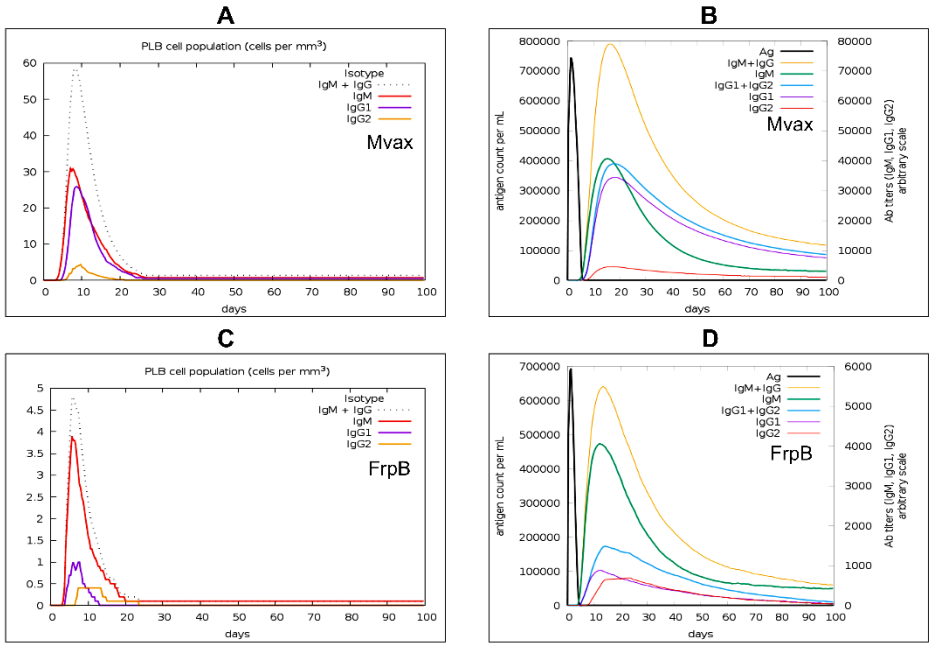

Figure 10. Predicted plasma cell and antibody responses over 100 days following a single dose of Mvax or FrpB. A. Plasma B-lymphocyte counts by isotype (IgM, IgG1, IgG2) in response to Mvax. **B.** Antigen clearance and immunoglobulin levels (subdivided by isotype) following a single dose of Mvax. **C.** Plasma B-lymphocyte counts by isotype in response to FrpB. **D.** Antigen clearance and immunoglobulin levels following a single dose of FrpB.

Discussion

The global burden of human brucellosis has risen sharply in recent years, with current estimates reaching approximately 2.1 million new cases annually [1]. Similar to other intracellular pathogens such as *Mycobacterium*, *Salmonella*, and *Listeria*, *Brucella* poses major therapeutic challenges due to the limited ability of most antibiotics to penetrate host cells and effectively reach its intracellular niches [13]. This concerning trend underscores the urgent need for safe and effective vaccine development as a critical strategy to prevent brucellosis and overcome the limitations of antibiotic-based treatments.

Using a reverse vaccinology strategy, this study introduces Mvax as a promising antivirulence multiepitope vaccine candidate for human brucellosis. The outer membrane protein FrpB was prioritized as a vaccine target based on both the in silico analyses conducted in this study and supporting evidence from prior research highlighting its role in *Brucella* virulence and immunogenicity [74–76].

Although previous studies have used FrpB (or its orthologue BhuA) in multiepitope *Brucella* vaccine designs [24,87], they relied on epitope sets that differ entirely from those selected here. Specifically, the present vaccine construct, Mvax, focuses on Th1 and IgM inducing epitopes and incorporates seven carefully selected peptides representing ~15.1% of the native FrpB sequence (100 of 661 amino acids). These epitopes were selected for their strong predicted binding affinities to immune receptors, high antigenicity, and lack of predicted toxicity. Because IFN-γ is a critical cytokine for host control of *Brucella* infection [85], an additional selection filter was applied to prioritize T-cell epitopes capable of inducing strong interferon responses. $CD4^+$ T cells are the primary source of IFN-γ during brucellosis, although $CD8^+$ T cells and other subsets also contribute [88]. Accordingly, both MHC-I and MHC-II interferon-inducing epitopes were preferentially selected for

 doi:10.20944/preprints202512.0403.v1

the vaccine design. Each epitope was individually docked to its corresponding immune receptor prior to Mvax assembly, demonstrating favorable binding energies consistent with potentially efficient immune recognition. For B-cell epitopes, an IgM-isotype B-cell receptor was used to ensure high predicted affinity for membrane-bound IgM, with the specific aim of promoting *Brucella*-specific IgM responses. Following epitope prioritization, different selected epitopes were strategically linked using a combination of flexible and rigid linkers including EAAAK, KK, AAY, and GPGPG [54–56]. To enhance immunogenicity, human β-defensin-3 (hBD-3), an endogenous antimicrobial peptide with potent adjuvant activity, was fused to the N-terminus of the first B-cell epitope as a built-in adjuvant. In vaccine designs, hBD-3 is favored as an adjuvant because it enhances antigen uptake and presentation, drives phenotypic maturation of dendritic cells, and promotes a Th1-skewed response with increased IFN-γ production, which is critical for effective protective cellular immunity [57,89–92].

For docking Mvax to immune receptors, TLR4 and TLR2/TLR6 were selected due to their well-documented roles in recognizing pathogen-associated molecular patterns and mediating immune resistance against *Brucella* infection [70]. TLR4 primarily recognizes lipopolysaccharides from Gram-negative bacteria like *Brucella*, while TLR2 forms heterodimers with TLR6 to detect lipoproteins and glycolipids, triggering downstream signaling pathways critical for host defense [70].

Human simulation analysis indicated a single dose of Mvax outperformed the parent FrpB protein in silico, inducing higher frequencies of memory T cells and increased levels of IL-12, IFN-γ, and IL-2, in line with a robust Th1- cell response. IL-12 plays a critical role in *Brucella* infection by driving Th1 differentiation, promoting IFN-γ production from CD4+/CD8+ T cells and NK cells, and activating macrophages for intracellular killing via iNOS upregulation [93]. IL-2 plays a key role in brucellosis immunity by promoting Th1 cell proliferation/differentiation and enhancing CD8+ T-cell and NK cell cytotoxicity against intracellular *Brucella* [85]. The predicted ability of Mvax to induce long-term Th1 immunity and high IFN-γ levels is promising but requires experimental validation, given that arming the host's mucosal immune defenses with resident memory T cells (TRMs) while expanding IFN-γ sources can prevent *Brucella* dissemination from the initial infection site to systemic tissue [94],

Notably, Mvax elicited approximately a 7.7-fold increase in IgM-isotype plasma cells accompanied by 10-fold higher IgM levels relative to native FrpB, indicating strong humoral activation. Current understanding from human studies on brucellosis primarily focuses on IgM as a diagnostic marker of acute/recent infection rather than a defined protective mechanism [95,96]. Nonetheless, our recent studies have shown that S19 vaccine-elicited secretory IgM plays a critical role in limiting early dissemination of virulent *Brucella melitensis* during the first two weeks after challenge, largely through complement activation, as evidenced by markedly higher splenic bacterial burdens in IgM-deficient vaccinated mice [26]. These findings, together with Mvax's demonstrated predicted capacity to induce strong Th1 responses and durable T-cell memory, underscore its ability to potentially coordinate potent humoral and cellular immunity.

Conclusion

This in silico study presents Mvax as a promising multiepitope vaccine candidate targeting *Brucella* virulence through high affinity, immunodominant epitopes. Immune simulations predict that Mvax elicits a robust Th1 cell response, characterized by activation of Th1 cells, memory formation, and cytokine production including IL-12, IFN-γ, and IL-2, which are critical for macrophage activation and intracellular bacterial clearance. Additionally, Mvax shows strong predicted induction of IgM, contributing to humoral immunity that may limit early *Brucella* dissemination and complement Th1-mediated protection. While experimental validation through in *vitro*, in *vivo*, and clinical studies is necessary, these in silico findings position Mvax as a next-generation vaccine candidate with the potential to provide effective protection against human brucellosis, mimicking key protective features of live-attenuated vaccines in a safer, rationally designed format.

 doi:10.20944/preprints202512.0403.v1

Supplementary Materials: The following supporting information can be downloaded at the website of this paper posted on Preprints.org, Supplementary Spreadsheet S1: NCBI-Retrieved Identical *Brucella* FrpB Sequences (Accession Numbers); Supplementary Spreadsheet S2: Global Population Coverage Estimates for Selected T cell Epitopes.

Author Contributions: MFA contributed 100% to this work.

Funding: MFA is funded by NIH (Project Number: R21AI185488).

Institutional Review Board Statement: Not applicable.

Informed Consent Statement: Not applicable.

Data Availability Statement: The data used and analyzed for this study are available from the corresponding author on reasonable request.

Conflicts of Interest: The author declares no conflicts of interest.

Abbreviations

The following abbreviations are used in this manuscript:

IEDB	Immune Epitope Database
NCBI	National Center for Biotechnology Information
MHCI	Major Histocompatibility Complex Class I
MHCII	Major Histocompatibility Complex Class II
PAMPs	Pathogen-Associated Molecular Patterns
IFN-γ	Interferon-gamma
Th	T helper cell
FrpB	Iron-regulated outer membrane protein
hBD-3	human β-defensin-3
Mvax	Multiepitope vaccine construct
HLA	Human Leukocyte Antigen
CTL	Cytotoxic T Lymphocyte
HTL	Helper T Lymphocyte
CD4	Cluster of Differentiation 4 (T helper cell marker)
CD8	*Cluster of Differentiation 8 (Cytotoxic T cell marker)*
TLR2	Toll-Like Receptor 2
TLR4	Toll-Like Receptor 4
TLR6	Toll-Like Receptor 6
IL-12	Interleukin-12
IL-2	Interleukin-2
IgM	Immunoglobulin M
sIgM	Secretory IgM
IgG	Immunoglobulin G
BCR	B Cell Receptor

References

1. Laine, C.G.; Johnson, V.E.; Scott, H.M.; Arenas-Gamboa, A.M. Global Estimate of Human Brucellosis Incidence - Volume 29, Number 9—September 2023 - Emerging Infectious Diseases Journal - CDC. *Emerg Infect Dis* **2023**, *29*, 1789–1797, doi:10.3201/EID2909.230052.
2. L'Hôte, L.; Light, I.; Mattiangeli, V.; Teasdale, M.D.; Halpin, Á.; Gourichon, L.; Key, F.M.; Daly, K.G. An 8000 Years Old Genome Reveals the Neolithic Origin of the Zoonosis Brucella Melitensis. *Nature Communications 2024 15:1* **2024**, *15*, 6132-, doi:10.1038/s41467-024-50536-1.
3. Gomez, G.; Adams, L.G.; Rice-Ficht, A.; Ficht, T.A. Host-Brucella Interactions and the Brucella Genome as Tools for Subunit Antigen Discovery and Immunization against Brucellosis. *Front Cell Infect Microbiol* **2013**, *4*, 38949, doi:10.3389/FCIMB.2013.00017/FULL.

 doi:10.20944/preprints202512.0403.v1

4. Pereira, C.R.; de Almeida, J.V.F.C.; de Oliveira, I.R.C.; de Oliveira, L.F.; Pereira, L.J.; Zangerônimo, M.G.; Lage, A.P.; Dorneles, E.M.S. Occupational Exposure to Brucella Spp.: A Systematic Review and Meta-Analysis. *PLoS Negl Trop Dis* **2020**, *14*, e0008164, doi:10.1371/JOURNAL.PNTD.0008164.
5. Qureshi, K.A.; Parvez, A.; Fahmy, N.A.; Abdel Hady, B.H.; Kumar, S.; Ganguly, A.; Atiya, A.; Elhassan, G.O.; Alfadly, S.O.; Parkkila, S.; et al. Brucellosis: Epidemiology, Pathogenesis, Diagnosis and Treatment–a Comprehensive Review. *Ann Med* **2024**, *55*, 2295398, doi:10.1080/07853890.2023.2295398.
6. Abdelbaset, A.E.; Abushahba, M.F.N.; Hamed, M.I.; Rawy, M.S. Sero-Diagnosis of Brucellosis in Sheep and Humans in Assiut and El-Minya Governorates, Egypt. *Int J Vet Sci Med* **2018**, *6*, S63–S67, doi:10.1016/j.ijvsm.2018.01.007.
7. Hasanjani Roushan, M.R.; Moulana, Z.; Mohseni Afshar, Z.; Ebrahimpour, S. Risk Factors for Relapse of Human Brucellosis. *Glob J Health Sci* **2015**, *8*, 77–82, doi:10.5539/gjhs.v8n7p77.
8. Lu, P.; Luo, B.; Wang, Q.; Wang, L.; Chen, M.; Jia, J.; Yang, M.; Pan, J.; Liu, J.; Li, Z. Progress in Brucellosis Immune Regulation Inflammatory Mechanisms and Diagnostic Advances. *Eur J Med Res* **2025**, *30*, 830, doi:10.1186/S40001-025-03068-3.
9. Guo, X.; Zeng, H.; Li, M.; Xiao, Y.; Gu, G.; Song, Z.; Shuai, X.; Guo, J.; Huang, Q.; Zhou, B.; et al. The Mechanism of Chronic Intracellular Infection with Brucella Spp. *Front Cell Infect Microbiol* **2023**, *13*, 1129172, doi:10.3389/FCIMB.2023.1129172.
10. Dadelahi, A.S.; Abushahba, M.F.N.; Ponzilacqua-Silva, B.; Chambers, C.A.; Moley, C.R.; Lacey, C.A.; Dent, A.L.; Skyberg, J. Interactions between B Cells and T Follicular Regulatory Cells Enhance Susceptibility to Brucella Infection Independent of the Anti-Brucella Humoral Response. *PLoS Pathog* **2023**, *19*, e1011672, doi:10.1371/JOURNAL.PPAT.1011672.
11. Dadelahi, A.S.; Lacey, C.A.; Chambers, C.A.; Ponzilacqua-Silva, B.; Skyberg, J.A. B Cells Inhibit CD4+ T Cell-Mediated Immunity to Brucella Infection in a Major Histocompatibility Complex Class II-Dependent Manner. *Infect Immun* **2020**, *88*, e00075-20, doi:10.1128/IAI.00075-20.
12. Goenka, R.; Guirnalda, P.D.; Black, S.J.; Baldwin, C.L. B Lymphocytes Provide an Infection Niche for Intracellular Bacterium Brucella Abortus. *Journal of Infectious Diseases* **2012**, *206*, doi:10.1093/infdis/jis310.
13. Abushahba, M.F.N.; Mohammad, H.; Thangamani, S.; Hussein, A.A.A.; Seleem, M.N. Impact of Different Cell Penetrating Peptides on the Efficacy of Antisense Therapeutics for Targeting Intracellular Pathogens. *Sci Rep* **2016**, *6*, 1–12, doi:10.1038/srep20832.
14. Perkins, S.D.; Smither, S.J.; Atkins, H.S. Towards a Brucella Vaccine for Humans. *FEMS Microbiol Rev* **2010**, *34*, 379–394, doi:10.1111/J.1574-6976.2010.00211.X.
15. Arenas-Gamboa, A.M.; Rice-Ficht, A.C.; Fan, Y.; Kahl-McDonagh, M.M.; Ficht, T.A. Extended Safety and Efficacy Studies of the Attenuated Brucella Vaccine Candidates 16MΔvjbR and S19ΔvjbR in the Immunocompromised IRF-1 -/- Mouse Model. *Clinical and Vaccine Immunology* **2012**, *19*, 249–260, doi:10.1128/CVI.05321-11;REQUESTEDJOURNAL:JOURNAL:CVI;ISSUE:ISSUE:DOI.
16. Vives-Soto, M.; Puerta-García, A.; Rodríguez-Sánchez, E.; Pereira, J.; Solera, J. What Risk Do Brucella Vaccines Pose to Humans? A Systematic Review of the Scientific Literature on Occupational Exposure. *PLoS Negl Trop Dis* **2024**, *18*, e0011889, doi:10.1371/JOURNAL.PNTD.0011889.
17. Avila-Calderón, E.D.; Lopez-Merino, A.; Sriranganathan, N.; Boyle, S.M.; Contreras-Rodríguez, A. A History of the Development of Brucella Vaccines. *Biomed Res Int* **2013**, *2013*, 743509, doi:10.1155/2013/743509.
18. Goodswen, S.J.; Kennedy, P.J.; Ellis, J.T. A Guide to Current Methodology and Usage of Reverse Vaccinology towards in Silico Vaccine Discovery. *FEMS Microbiol Rev* **2023**, *47*, doi:10.1093/FEMSRE/FUAD004.
19. Vishnu, U.S.; Sankarasubramanian, J.; Gunasekaran, P.; Rajendhran, J. Identification of Potential Antigens from Non-Classically Secreted Proteins and Designing Novel Multitope Peptide Vaccine Candidate against Brucella Melitensis through Reverse Vaccinology and Immunoinformatics Approach. *Infection, Genetics and Evolution* **2017**, *55*, 151–158, doi:10.1016/j.meegid.2017.09.015.
20. Chai, Z.L.; Qi, X.X.; Li, R.; Luo, J.R.; Li, C.; Shi, H.D.; Tian, T.T.; Shang, K.Y.; Zhu, Y.J.; Zhang, F.B. Reverse Vaccinology-Driven Construction and Bioinformatics Validation of a Multi-Epitope Vaccine against Brucella Spp. *Scientific Reports 2025 15:1* **2025**, *15*, 36663-, doi:10.1038/s41598-025-20507-7.

21. Gharazi, H.; Doosti, A.; Abdizadeh, R. Brucellosis Novel Multi-Epitope Vaccine Design Based on in Silico Analysis Focusing on Brucella Abortus. *BMC Immunol* **2025**, *26*, 46, doi:10.1186/S12865-025-00728-1.
22. Molina, R.E.; Osorio, A.; Flores-Concha, M.; Gómez, L.A.; Alvarado, I.; Ferrari, I.; Oñate, A. Immunoinformatic Design of a Multivalent Vaccine against Brucella Abortus and Its Evaluation in a Murine Model Using a DNA Prime-Protein Boost Strategy. *Front Immunol* **2024**, *15*, 1456078, doi:10.3389/FIMMU.2024.1456078.
23. Shi, J.; Zhu, Y.; Yin, Z.; He, Y.; Li, Y.; Haimiti, G.; Xie, X.; Niu, C.; Guo, W.; Zhang, F. In Silico Designed Novel Multi-Epitope MRNA Vaccines against Brucella by Targeting Extracellular Protein BtuB and LptD. *Scientific Reports 2024 14:1* **2024**, *14*, 7278-, doi:10.1038/s41598-024-57793-6.
24. Hameed, A.R.; Mohammed, B.Q.; Jassim, T.S.; Alharbi, M.; Ahmad, S. Design of a Novel Multi-Epitopes Based Vaccine against Brucellosis. *Inform Med Unlocked* **2023**, *39*, 101276, doi:10.1016/J.IMU.2023.101276.
25. Abushahba, M.F.; Dadelahi, A.S.; Lemoine, E.L.; Skyberg, J.A.; Vyas, S.; Dhoble, S.; Ghodake, V.; Patravale, V.B.; Adamovicz, J.J. Safe Subunit Green Vaccines Confer Robust Immunity and Protection against Mucosal Brucella Infection in Mice. *Vaccines 2023, Vol. 11, Page 546* **2023**, *11*, 546, doi:10.3390/VACCINES11030546.
26. Abushahba, M.F.N.; Dadelahi, A.S.; Ponzilacqua-Silva, B.; Moley, C.R.; Skyberg, J.A. Contrasting Roles for IgM and B-Cell MHCII Expression in Brucella Abortus S19 Vaccine-Mediated Efficacy against B. Melitensis Infection. *mSphere* **2024**, *9*, doi:10.1128/MSPHERE.00750-23.
27. Teufel, F.; Almagro Armenteros, J.J.; Johansen, A.R.; Gíslason, M.H.; Pihl, S.I.; Tsirigos, K.D.; Winther, O.; Brunak, S.; von Heijne, G.; Nielsen, H. SignalP 6.0 Predicts All Five Types of Signal Peptides Using Protein Language Models. *Nat Biotechnol* **2022**, *40*, 1023, doi:10.1038/S41587-021-01156-3.
28. Chen, C.; Xu, Y.; Ouyang, J.; Xiong, X.; Łabaj, P.P.; Chmielarczyk, A.; Różańska, A.; Zhang, H.; Liu, K.; Shi, T.; et al. VirulentHunter: Deep Learning-Based Virulence Factor Predictor Illuminates Pathogenicity in Diverse Microbial Contexts. *Brief Bioinform* **2025**, *26*, doi:10.1093/BIB/BBAF271.
29. Garg, A.; Gupta, D. VirulentPred: A SVM Based Prediction Method for Virulent Proteins in Bacterial Pathogens. *BMC Bioinformatics 2008 9:1* **2008**, *9*, 62-, doi:10.1186/1471-2105-9-62.
30. Yu, C.; Lin, C.; Hwang, J. Predicting Subcellular Localization of Proteins for Gram-Negative Bacteria by Support Vector Machines Based on n-Peptide Compositions. *Protein Sci* **2004**, *13*, 1402–1406, doi:10.1110/PS.03479604.
31. Moreno, J.; Nielsen, H.; Winther, O.; Teufel, F. Predicting the Subcellular Location of Prokaryotic Proteins with DeepLocPro. *Bioinformatics* **2024**, *40*, doi:10.1093/BIOINFORMATICS/BTAE677.
32. Tsirigos, K.D.; Peters, C.; Shu, N.; Käll, L.; Elofsson, A. The TOPCONS Web Server for Consensus Prediction of Membrane Protein Topology and Signal Peptides. *Nucleic Acids Res* **2015**, *43*, W401–W407, doi:10.1093/NAR/GKV485.
33. Reynisson, B.; Alvarez, B.; Paul, S.; Peters, B.; Nielsen, M. NetMHCpan-4.1 and NetMHCIIpan-4.0: Improved Predictions of MHC Antigen Presentation by Concurrent Motif Deconvolution and Integration of MS MHC Eluted Ligand Data. *Nucleic Acids Res* **2020**, *48*, W449–W454, doi:10.1093/NAR/GKAA379.
34. Erik, J.; Larsen, P.; Lund, O.; Nielsen, M. Improved Method for Predicting Linear B-Cell Epitopes. *Immunome Research 2006 2:1* **2006**, *2*, 2-, doi:10.1186/1745-7580-2-2.
35. Greenbaum, J.; Sidney, J.; Chung, J.; Brander, C.; Peters, B.; Sette, A. Functional Classification of Class II Human Leukocyte Antigen (HLA) Molecules Reveals Seven Different Supertypes and a Surprising Degree of Repertoire Sharing across Supertypes. *Immunogenetics* **2011**, *63*, 325–335, doi:10.1007/S00251-011-0513-0.
36. Moutaftsi, M.; Peters, B.; Pasquetto, V.; Tscharke, D.C.; Sidney, J.; Bui, H.H.; Grey, H.; Sette, A. A Consensus Epitope Prediction Approach Identifies the Breadth of Murine T(CD8+)-Cell Responses to Vaccinia Virus. *Nat Biotechnol* **2006**, *24*, 817–819, doi:10.1038/NBT1215.
37. Kotturi, M.F.; Peters, B.; Buendia-Laysa, F.; Sidney, J.; Oseroff, C.; Botten, J.; Grey, H.; Buchmeier, M.J.; Sette, A. The CD8+ T-Cell Response to Lymphocytic Choriomeningitis Virus Involves the L Antigen: Uncovering New Tricks for an Old Virus. *J Virol* **2007**, *81*, 4928–4940, doi:10.1128/JVI.02632-06.
38. Doytchinova, I.A.; Flower, D.R. VaxiJen: A Server for Prediction of Protective Antigens, Tumour Antigens and Subunit Vaccines. *BMC Bioinformatics* **2007**, *8*, doi:10.1186/1471-2105-8-4.
39. Gupta, S.; Kapoor, P.; Chaudhary, K.; Gautam, A.; Kumar, R.; Raghava, G.P.S. In Silico Approach for Predicting Toxicity of Peptides and Proteins. *PLoS One* **2013**, *8*, doi:10.1371/JOURNAL.PONE.0073957.

 doi:10.20944/preprints202512.0403.v1

40. Bui, H.H.; Sidney, J.; Li, W.; Fusseder, N.; Sette, A. Development of an Epitope Conservancy Analysis Tool to Facilitate the Design of Epitope-Based Diagnostics and Vaccines. *BMC Bioinformatics 2007 8:1* **2007**, *8*, 361-, doi:10.1186/1471-2105-8-361.
41. Murphy, E.A.; Sathiyaseelan, J.; Parent, M.A.; Zou, B.; Baldwin, C.L. Interferon-γ Is Crucial for Surviving a Brucella Abortus Infection in Both Resistant C57BL/6 and Susceptible BALB/c Mice. *Immunology* **2001**, *103*, 511, doi:10.1046/J.1365-2567.2001.01258.X.
42. Dhall, A.; Patiyal, S.; Raghava, G.P.S. A Hybrid Method for Discovering Interferon-Gamma Inducing Peptides in Human and Mouse. *Scientific Reports 2024 14:1* **2024**, *14*, 26859-, doi:10.1038/s41598-024-77957-8.
43. Bui, H.H.; Sidney, J.; Dinh, K.; Southwood, S.; Newman, M.J.; Sette, A. Predicting Population Coverage of T-Cell Epitope-Based Diagnostics and Vaccines. *BMC Bioinformatics 2006 7:1* **2006**, *7*, 153-, doi:10.1186/1471-2105-7-153.
44. Lai, S.; Chen, Q.; Li, Z. Human Brucellosis: An Ongoing Global Health Challenge. *China CDC Wkly* **2021**, *3*, 120, doi:10.46234/CCDCW2021.031.
45. Lamiable, A.; Thevenet, P.; Rey, J.; Vavrusa, M.; Derreumaux, P.; Tuffery, P. PEP-FOLD3: Faster de Novo Structure Prediction for Linear Peptides in Solution and in Complex. *Nucleic Acids Res* **2016**, *44*, W449–W454, doi:10.1093/NAR/GKW329.
46. Kozakov, D.; Hall, D.R.; Xia, B.; Porter, K.A.; Padhorny, D.; Yueh, C.; Beglov, D.; Vajda, S. The ClusPro Web Server for Protein–Protein Docking. *Nature Protocols 2017 12:2* **2017**, *12*, 255–278, doi:10.1038/nprot.2016.169.
47. Su, Q.; Chen, M.; Shi, Y.; Zhang, X.; Huang, G.; Huang, B.; Liu, D.; Liu, Z.; Shi, Y. Cryo-EM Structure of the Human IgM B Cell Receptor. *Science (1979)* **2022**, *377*, 875–880, doi:10.1126/SCIENCE.ABO3923;WEBSITE:WEBSITE:AAAS-SITE;JOURNAL:JOURNAL:SCIENCE;WGROUP:STRING:PUBLICATION.
48. Parry, C.S.; Gorski, J.; Stern, L.J. Crystallographic Structure of the Human Leukocyte Antigen DRA, DRB3*0101: Models of a Directional Alloimmune Response and Autoimmunity. *J Mol Biol* **2007**, *371*, 435–446, doi:10.1016/J.JMB.2007.05.025.
49. Gerstner, C.; Dubnovitsky, A.; Sandin, C.; Kozhukh, G.; Uchtenhagen, H.; James, E.A.; Rönnelid, J.; Ytterberg, A.J.; Pieper, J.; Reed, E.; et al. Functional and Structural Characterization of a Novel HLA-DRB1*04: 01-Restricted α-Enolase T Cell Epitope in Rheumatoid Arthritis. *Front Immunol* **2016**, *7*, 224418, doi:10.3389/FIMMU.2016.00494/BIBTEX.
50. Waterhouse, A.M.; Studer, G.; Robin, X.; Bienert, S.; Tauriello, G.; Schwede, T. The Structure Assessment Web Server: For Proteins, Complexes and More. *Nucleic Acids Res* **2024**, *52*, W318–W323, doi:10.1093/NAR/GKAE270.
51. Xue, L.C.; Rodrigues, J.P.; Kastritis, P.L.; Bonvin, A.M.; Vangone, A. PRODIGY: A Web Server for Predicting the Binding Affinity of Protein–Protein Complexes. *Bioinformatics* **2016**, *32*, 3676–3678, doi:10.1093/BIOINFORMATICS/BTW514.
52. Wang, J.; Youkharibache, P.; Zhang, D.; Lanczycki, C.J.; Geer, R.C.; Madej, T.; Phan, L.; Ward, M.; Lu, S.; Marchler, G.H.; et al. ICn3D, a Web-Based 3D Viewer for Sharing 1D/2D/3D Representations of Biomolecular Structures. *Bioinformatics* **2020**, *36*, 131–135, doi:10.1093/BIOINFORMATICS/BTZ502.
53. Wang, J.; Youkharibache, P.; Marchler-Bauer, A.; Lanczycki, C.; Zhang, D.; Lu, S.; Madej, T.; Marchler, G.H.; Cheng, T.; Chong, L.C.; et al. ICn3D: From Web-Based 3D Viewer to Structural Analysis Tool in Batch Mode. *Front Mol Biosci* **2022**, *9*, doi:10.3389/FMOLB.2022.831740.
54. Chen, X.; Zaro, J.L.; Shen, W.C. Fusion Protein Linkers: Property, Design and Functionality. *Adv Drug Deliv Rev* **2012**, *65*, 1357, doi:10.1016/J.ADDR.2012.09.039.
55. Livingston, B.; Crimi, C.; Newman, M.; Higashimoto, Y.; Appella, E.; Sidney, J.; Sette, A. A Rational Strategy to Design Multiepitope Immunogens Based on Multiple Th Lymphocyte Epitopes. *The Journal of Immunology* **2002**, *168*, 5499–5506, doi:10.4049/JIMMUNOL.168.11.5499.
56. Salahlou, R.; Farajnia, S.; Bargahi, N.; Bakhtiyari, N.; Elmi, F.; Shahgolzari, M.; Fiering, S.; Venkataraman, S. Development of a Novel Multi-epitope Vaccine against the Pathogenic Human Polyomavirus V6/7 Using Reverse Vaccinology. *BMC Infect Dis* **2024**, *24*, 177, doi:10.1186/S12879-024-09046-0.

57. Ferris, L.K.; Mburu, Y.K.; Mathers, A.R.; Fluharty, E.R.; Larregina, A.T.; Ferris, R.L.; Falo, L.D. Human Beta-Defensin 3 Induces Maturation of Human Langerhans Cell-like Dendritic Cells: An Antimicrobial Peptide That Functions as an Endogenous Adjuvant. *Journal of Investigative Dermatology* **2013**, *133*, 460–468, doi:10.1038/jid.2012.319.
58. Geourjon, C.; Deléage, G. SOPMA: Significant Improvements in Protein Secondary Structure Prediction by Consensus Prediction from Multiple Alignments. *Comput Appl Biosci* **1995**, *11*, 681–684, doi:10.1093/BIOINFORMATICS/11.6.681.
59. Combet, C.; Blanchet, C.; Geourjon, C.; Deléage, G. NPS@: Network Protein Sequence Analysis. *Trends Biochem Sci* **2000**, *25*, 147–150, doi:10.1016/S0968-0004(99)01540-6.
60. Du, Z.; Su, H.; Wang, W.; Ye, L.; Wei, H.; Peng, Z.; Anishchenko, I.; Baker, D.; Yang, J. The TrRosetta Server for Fast and Accurate Protein Structure Prediction. *Nat Protoc* **2021**, *16*, 5634–5651, doi:10.1038/S41596-021-00628-9.
61. Wiederstein, M.; Sippl, M.J. ProSA-Web: Interactive Web Service for the Recognition of Errors in Three-Dimensional Structures of Proteins. *Nucleic Acids Res* **2007**, *35*, doi:10.1093/NAR/GKM290.
62. Ko, J.; Park, H.; Heo, L.; Seok, C. GalaxyWEB Server for Protein Structure Prediction and Refinement. *Nucleic Acids Res* **2012**, *40*, doi:10.1093/NAR/GKS493.
63. Colovos, C.; Yeates, T.O. Verification of Protein Structures: Patterns of Nonbonded Atomic Interactions. *Protein Sci* **1993**, *2*, 1511–1519, doi:10.1002/PRO.5560020916.
64. Gasteiger, E.; Gattiker, A.; Hoogland, C.; Ivanyi, I.; Appel, R.D.; Bairoch, A. ExPASy: The Proteomics Server for in-Depth Protein Knowledge and Analysis. *Nucleic Acids Res* **2003**, *31*, 3784, doi:10.1093/NAR/GKG563.
65. Nguyen, M.N.; Krutz, N.L.; Limviphuvadh, V.; Lopata, A.L.; Gerberick, G.F.; Maurer-Stroh, S. AllerCatPro 2.0: A Web Server for Predicting Protein Allergenicity Potential. *Nucleic Acids Res* **2022**, *50*, W36, doi:10.1093/NAR/GKAC446.
66. Hebditch, M.; Carballo-Amador, M.A.; Charonis, S.; Curtis, R.; Warwicker, J. Protein–Sol: A Web Tool for Predicting Protein Solubility from Sequence. *Bioinformatics* **2017**, *33*, 3098–3100, doi:10.1093/BIOINFORMATICS/BTX345.
67. Ponomarenko, J.; Bui, H.H.; Li, W.; Fusseder, N.; Bourne, P.E.; Sette, A.; Peters, B. ElliPro: A New Structure-Based Tool for the Prediction of Antibody Epitopes. *BMC Bioinformatics* **2008**, *9*, 514, doi:10.1186/1471-2105-9-514.
68. Park, B.S.; Song, D.H.; Kim, H.M.; Choi, B.S.; Lee, H.; Lee, J.O. The Structural Basis of Lipopolysaccharide Recognition by the TLR4–MD-2 Complex. *Nature 2009 458:7242* **2009**, *458*, 1191–1195, doi:10.1038/nature07830.
69. Kang, J.Y.; Nan, X.; Jin, M.S.; Youn, S.J.; Ryu, Y.H.; Mah, S.; Han, S.H.; Lee, H.; Paik, S.G.; Lee, J.O. Recognition of Lipopeptide Patterns by Toll-like Receptor 2-Toll-like Receptor 6 Heterodimer. *Immunity* **2009**, *31*, 873–884, doi:10.1016/j.immuni.2009.09.018.
70. Yu, H.; Gu, X.; Wang, D.; Wang, Z. Brucella Infection and Toll-like Receptors. *Front Cell Infect Microbiol* **2024**, *14*, 1342684, doi:10.3389/FCIMB.2024.1342684.
71. Laubenbacher, R.; Adler, F.; An, G.; Castiglione, F.; Eubank, S.; Fonseca, L.L.; Glazier, J.; Helikar, T.; Jett-Tilton, M.; Kirschner, D.; et al. Toward Mechanistic Medical Digital Twins: Some Use Cases in Immunology. *Front Digit Health* **2024**, *6*, 1349595, doi:10.3389/FDGTH.2024.1349595/BIBTEX.
72. Rapin, N.; Lund, O.; Bernaschi, M.; Castiglione, F. Computational Immunology Meets Bioinformatics: The Use of Prediction Tools for Molecular Binding in the Simulation of the Immune System. *PLoS One* **2010**, *5*, e9862, doi:10.1371/JOURNAL.PONE.0009862.
73. Ong, E.; Cooke, M.F.; Huffman, A.; Xiang, Z.; Wong, M.U.; Wang, H.; Seetharaman, M.; Valdez, N.; He, Y. Vaxign2: The Second Generation of the First Web-Based Vaccine Design Program Using Reverse Vaccinology and Machine Learning. *Nucleic Acids Res* **2021**, *49*, W671–W678, doi:10.1093/NAR/GKAB279.
74. Paulley, J.T.; Anderson, E.S.; Roop, R.M. Brucella Abortus Requires the Heme Transporter BhuA for Maintenance of Chronic Infection in BALB/c Mice. *Infect Immun* **2007**, *75*, 5248, doi:10.1128/IAI.00460-07.
75. Avila-Caldern, E.D.; Lopez-Merino, A.; Jain, N.; Peralta, H.; Lpez-Villegas, E.O.; Sriranganathan, N.; Boyle, S.M.; Witonsky, S.; Contreras-Rodríguez, A. Characterization of Outer Membrane Vesicles from Brucella Melitensis and Protection Induced in Mice. *J Immunol Res* **2012**, *2012*, 352493, doi:10.1155/2012/352493.

76. Sadeghi, Z.; Fasihi-Ramandi, M.; Bouzari, S. Brucella Antigens (BhuA, 7α-HSDH, FliC) in Poly I:C Adjuvant as Potential Vaccine Candidates against Brucellosis. *J Immunol Methods* **2022**, *500*, 113172, doi:10.1016/J.JIM.2021.113172.
77. Jain, N.; Shankar, U.; Majee, P.; Kumar, A. Scrutinizing the SARS-CoV-2 Protein Information for Designing an Effective Vaccine Encompassing Both the T-Cell and B-Cell Epitopes. *Infection, Genetics and Evolution* **2020**, *87*, 104648, doi:10.1016/J.MEEGID.2020.104648.
78. Giri-Rachman, E.A.; Kurnianti, A.M.F.; Rizarullah; Setyadi, A.H.; Artarini, A.; Tan, M.I.; Riani, C.; Natalia, D.; Aditama, R.; Nugrahapraja, H. An Immunoinformatics Approach in Designing High-Coverage MRNA Multi-Epitope Vaccine against Multivariant SARS-CoV-2. *Journal of Genetic Engineering & Biotechnology* **2025**, *23*, 100524, doi:10.1016/J.JGEB.2025.100524.
79. Kolla, H.B.; Tirumalasetty, C.; Sreerama, K.; Ayyagari, V.S. An Immunoinformatics Approach for the Design of a Multi-Epitope Vaccine Targeting Super Antigen TSST-1 of Staphylococcus Aureus. *Journal of Genetic Engineering and Biotechnology* **2021**, *19*, 69, doi:10.1186/S43141-021-00160-Z.
80. Manocha, N.; Laubreton, D.; Robert, X.; Marvel, J.; Gueguen-Chaignon, V.; Gouet, P.; Kumar, P.; Khanna, M. Unveiling a Shield of Hope: A Novel Multiepitope-Based Immunogen for Cross-Serotype Cellular Defense against Dengue Virus. *Vaccines (Basel)* **2024**, *12*, 316, doi:10.3390/VACCINES12030316/S1.
81. Bahadori, Z.; Shafaghi, M.; Madanchi, H.; Ranjbar, M.M.; Shabani, A.A.; Mousavi, S.F. In Silico Designing of a Novel Epitope-Based Candidate Vaccine against Streptococcus Pneumoniae with Introduction of a New Domain of PepO as Adjuvant. *Journal of Translational Medicine 2022 20:1* **2022**, *20*, 389-, doi:10.1186/S12967-022-03590-6.
82. Du, X.; Li, Y.; Xia, Y.L.; Ai, S.M.; Liang, J.; Sang, P.; Ji, X.L.; Liu, S.Q. Insights into Protein–Ligand Interactions: Mechanisms, Models, and Methods. *Int J Mol Sci* **2016**, *17*, 144, doi:10.3390/IJMS17020144.
83. Puagsopa, J.; Jumpalee, P.; Dechanun, S.; Choengchalad, S.; Lohasupthawee, P.; Sutjaritvorakul, T.; Meksiriporn, B. Development of a Broad-Spectrum Pan-Mpox Vaccine via Immunoinformatic Approaches. *International Journal of Molecular Sciences 2025, Vol. 26, Page 7210* **2025**, *26*, 7210, doi:10.3390/IJMS26157210.
84. Xu, G.; Zhang, P.; Dang, R.; Jiang, Y.; Wang, F.; Wang, B.; Yang, M. Dynamic Changes of Th1 Cytokines and the Clinical Significance of the IFN-γ/TNF-α Ratio in Acute Brucellosis. *Mediators Inflamm* **2019**, *2019*, 5869257, doi:10.1155/2019/5869257.
85. Skendros, P.; Pappas, G.; Boura, P. Cell-Mediated Immunity in Human Brucellosis. *Microbes Infect* **2011**, *13*, 134–142, doi:10.1016/J.MICINF.2010.10.015.
86. Annunziato, F.; Romagnani, S. Heterogeneity of Human Effector CD4+ T Cells. *Arthritis Res Ther* **2009**, *11*, doi:10.1186/AR2843.
87. Sadeghi, Z.; Fasihi-Ramandi, M.; Bouzari, S. Evaluation of Immunogenicity of Novel Multi-Epitope Subunit Vaccines in Combination with Poly I:C against Brucella Melitensis and Brucella Abortus Infection. *Int Immunopharmacol* **2019**, *75*, doi:10.1016/J.INTIMP.2019.105829.
88. Brandão, A.P.M.S.; Oliveira, F.S.; Carvalho, N.B.; Vieira, L.Q.; Azevedo, V.; MacEdo, G.C.; Oliveira, S.C. Host Susceptibility to Brucella Abortus Infection Is More Pronounced in IFN-γ Knockout than IL-12/B2-Microglobulin Double-Deficient Mice. *J Immunol Res* **2012**, *2012*, 589494, doi:10.1155/2012/589494.
89. Tewary, P.; de la Rosa, G.; Sharma, N.; Rodriguez, L.G.; Tarasov, S.G.; Howard, O.M.Z.; Shirota, H.; Steinhagen, F.; Klinman, D.M.; Yang, D.; et al. β-Defensin 2 and 3 Promote the Uptake of Self or CpG DNA, Enhance IFN-α Production by Human Plasmacytoid Dendritic Cells, and Promote Inflammation. *The Journal of Immunology* **2013**, *191*, 865–874, doi:10.4049/JIMMUNOL.1201648.
90. Yang, H.; Lei, X.; Chai, S.; Zhang, S.; Su, G.; Du, L. A Multi-Epitope Vaccine Incorporating Adhesin-Derived Antigens Protects against Mycobacterium Tuberculosis Infection and Dissemination. *Front Immunol* **2025**, *16*, 1707471, doi:10.3389/FIMMU.2025.1707471.
91. Malgwi, S.A.; Adeleke, V.T.; Adeleke, M.A.; Okpeku, M. Multi-Epitope Based Peptide Vaccine Candidate Against Babesia Infection From Rhoptry-Associated Protein 1 (RAP-1) Antigen Using Immuno-Informatics: An In Silico Approach. *Bioinform Biol Insights* **2024**, *18*, 11779322241287114, doi:10.1177/11779322241287114.
92. Martinelli, D.D. In Silico Vaccine Design: A Tutorial in Immunoinformatics. *Healthcare Analytics* **2022**, *2*, 100044, doi:10.1016/J.HEALTH.2022.100044.

 doi:10.20944/preprints202512.0403.v1

93. Zhan, Y.; Liu, Z.; Cheers, C. Tumor Necrosis Factor Alpha and Interleukin-12 Contribute to Resistance to the Intracellular Bacterium Brucella Abortus by Different Mechanisms. *Infect Immun* **1996**, *64*, 2782–2786, doi:10.1128/IAI.64.7.2782-2786.1996.
94. Pascual, D.W.; Goodwin, Z.I.; Bhagyaraj, E.; Hoffman, C.; Yang, X. Activation of Mucosal Immunity as a Novel Therapeutic Strategy for Combating Brucellosis. *Front Microbiol* **2022**, *13*, 1018165, doi:10.3389/FMICB.2022.1018165/FULL.
95. Avijgan, M.; Rostamnezhad, M.; Jahanbani-Ardakani, H. Clinical and Serological Approach to Patients with Brucellosis: A Common Diagnostic Dilemma and a Worldwide Perspective. *Microb Pathog* **2019**, *129*, 125–130, doi:10.1016/J.MICPATH.2019.02.011.
96. Solís García del Pozo, J.; Lorente Ortuño, S.; Navarro, E.; Solera, J. Detection of IgM Antibrucella Antibody in the Absence of IgGs: A Challenge for the Clinical Interpretation of Brucella Serology. *PLoS Negl Trop Dis* **2014**, *8*, e3390, doi:10.1371/JOURNAL.PNTD.0003390.